https://doi.org/10.5194/egusphere-2026-1404
Preprint. Discussion started: 30 March 2026

Evaluation and improvement of CAMS-derived CCN number concentrations using in-situ measurements

Yannick Emanuel Anders[1], Karoline Block[1], Mira Pöhlker[1,2], and Johannes Quaas[1]

[1]Leipzig Institute for Meteorology, Faculty of Physics and Earth System Sciences, Leipzig University, 04103 Leipzig, Germany
[2]Department of Atmospheric Microphysics, Leibniz Institute for Tropospheric Research (TROPOS), 04318 Leipzig, Germany

Correspondence: Karoline Block (karoline.block@uni-leipzig.de)

Abstract. Cloud condensation nuclei (CCN) are essential components of aerosol-cloud interactions (ACI). Thus, a precise knowledge about their number concentrations (Nccn) is crucial for climate models and ACI studies. This study presents a comprehensive evaluation of the recently published CAMS-derived total Nccn using direct observations from 25 ground-based sites. The analysis specifically focuses on the temporal variability, the applicability of CAMS-derived Nccn across different environments and pollution regimes and in particular, the sensitivity of CCN to supersaturation. For the latter aspect, a bias shift is identified in simulated Nccn that correlates to the ratio of the two dominant CCN species, likely reflecting assumptions in the underlying size distributions and/or emissions fractions. To address this issue, we developed an observation-based parametrization that is applied to CAMS-derived total Nccn without modifying aerosol size distributions or species concentrations. This approach substantially reduces biases leading the way to an improved version of CAMS-derived Nccn.

1 Introduction

The simulation of aerosol-cloud interactions (ACI), still a remaining source of uncertainty in climate model intercomparisons (IPCC, 2023), relies on accurate fields of cloud condensation nuclei (CCN) number concentrations (Nccn) (e.g., Seinfeld et al., 2016). Since direct observations of CCN are only possible through in-situ measurements, from ground-based facilities, air- and shipborne platforms, the spatial and temporal distribution of observed Nccn is still sparse. For that reason, most climate models and ACI studies incorporate aerosol optical properties, e.g., aerosol optical depth (AOD), as a proxy for Nccn (e.g., Quaas et al., 2020; Gryspeerdt and Stier, 2012; Bellouin et al., 2020). Derived from satellite measurements, AOD data can potentially be provided on a global domain, continuously over long time periods. However, the use of AOD as an estimate of Nccn comes with disadvantages (e.g., Stier, 2016; Jia et al., 2021): As a column-integrated optical variable, it can neither account for the vertical variability of CCN nor the variety of aerosol species that can act as CCN, depending on their size and hygroscopicity. Also, other aerosol processes, such as swelling, might result in changes in the AOD, which are not caused by changes in the number of CCN (e.g., Quaas et al., 2009). Challenges in the satellite retrieval above cloudy or other bright surfaces reduce the global presentability of AOD as a CCN proxy. For example, Stier (2016) stated that the variability in AOD explains only 25 % of global CCN variance.

https://doi.org/10.5194/egusphere-2026-1404
Preprint. Discussion started: 30 March 2026

Thus, other approaches for the determination of globally resolved Nccns have been proposed. One of them is the recently published dataset by Block (2023), where Nccn are derived from aerosol mass mixing ratios from the Copernicus Atmosphere Monitoring Service (CAMS) aerosol reanalysis (Inness et al., 2019). The CAMS-derived CCN dataset contains globally and vertically resolved Nccn for 6 supersaturations ranging from 0.1 % to 1 %.

This dataset has been used in several studies but has received little systematic evaluation. In a first very brief evaluation, Block et al. (2024) compared CAMS Nccn and ground-based Nccn observations from five measurement sites at a single supersaturation of 0.4 %. Considering all data points, they found an improved overall correlation coefficient of 0.71, compared to the use of a Moderate Resolution Imaging Spectroradiometer (MODIS; Levy et al., 2013) AOD product as a CCN proxy, which yielded an overall correlation coefficient of 0.37. They have also found that observations are overestimated in their median and interquartile range for four out of five stations at this supersaturation. Notably, the largest bias has been obtained for the station with the highest CCN concentration. Whether this behavior is common to heavily polluted sites in general, has not been confirmed yet, as other sites with a similar level of pollution have not been validated yet.

A recent study by Kulkarni et al. (2025) examined the vertical distribution of CAMS-derived Nccn and compared it to airborne Nccn measurements that have been performed over the Southern Great Plains. For both sampling periods in spring and summer, they found that CAMS-derived Nccn tends to underestimate the observations. The r^2 coefficients of determination were 0.54 and 0.31, respectively for the two periods. The underestimation was found to be strongest at higher Nccn ($\geq$1400 cm^{-3}), where the authors obtained an underprediction by a factor of 8. Also in comparison to other CCN simulating methods, CAMS-derived Nccn exhibit the lowest concentrations in the scope of this specific study.

A similar result has been found by Choudhury et al. (2025), but for data points below an altitude of 2 km and only for a single supersaturation of 0.2 %. They compared the spatio-temporal variability of CAMS-derived Nccn to another novel global CCN dataset, which has been derived from Cloud Aerosol Lidar with Orthogonal Polarization (CALIOP) measurements (Choudhury and Tesche, 2023). Overall, CALIOP-derived Nccn are 79 % higher than CAMS-derived Nccn. Their analysis revealed that the largest discrepancies were found over the oceans, especially in the southern hemisphere (SH), while over the northern hemisphere (NH), the differences between the medians of CALIOP and CAMS are smaller. For all oceanic domains, except North Atlantic, both datasets furthermore disagree on the representation of the respective seasonal cycle, while the patterns in continental regions are mostly consistent. They have also found that inter-hemispheric differences are larger in CAMS than in CALIOP.

All of the mentioned studies only focused on one single supersaturation each: 0.2 % (Choudhury et al., 2025), 0.24 % (Kulkarni et al., 2025) and 0.4 % (Block et al., 2024). In contrast, Anders et al. (2025) made use of all 6 available supersaturations in their comparison of CAMS-derived Nccn to 13 measurement sites in both continental and marine environment. For most sites they found a supersaturation between 0.4 % and 0.8 % showing the best agreement between CAMS-derived CCN and observations. At some stations, higher supersaturations are less biased, while at others, low supersaturations perform better, which confirms the regional inhomogeneity that was found by Choudhury et al. (2025). Furthermore, Anders et al. (2025) revealed that CAMS-derived Nccn tend to underestimate at low supersaturations while it tends to overestimate at high supersaturations.

https://doi.org/10.5194/egusphere-2026-1404
Preprint. Discussion started: 30 March 2026

The bias shift identified in that study motivated the present work, which provides a substantially more extensive analysis of the CCN-supersaturation relationship in the CAMS-derived Nccn dataset, including and evaluation of its performance against an extended set of ground-based observational sites. Here we perform a systematic analysis on the variability of CAMS-derived total Nccn in time, its suitability in different environments and pollution regimes and in particular, its sensitivity to supersaturation.

2 Methodology

2.1 The CAMS-derived Nccn dataset

The Nccn dataset (Block, 2023) that is being evaluated in this study was derived from the Copernicus Atmosphere Monitoring Service (CAMS) reanalysis (Inness et al., 2019), which is produced using the Integrated Forcasting System (IFS; Morcrette et al., 2009; Rémy et al., 2019) of the European Centre for Medium-Range Weather Forecast (ECMWF) and its data assimilation scheme (Benedetti et al., 2009). The aerosol mass mixing ratios that are simulated by the IFS are constrained with aerosol optical depth (AOD) retrievals from satellite data. Incorporated are the dark target product and deep-blue product of MODIS as well as AOD data retrieved from the Advanced Along-Track Scanning Radiometer (AATSR; Popp et al., 2016). It has to be pointed out that the assimilation is limited to latitudes between 70° S and 70° N, due to the low solar illumination in polar regions (Inness et al., 2019). From these constrained aerosol mass mixing ratios, Block et al. (2024) have derived total and species-related Nccn using a simplified kappa-Köhler approach, assuming fixed hygroscopicity (kappa) values for each CCN-relevant aerosol species and globally fixed log-normal size distributions for each aerosol component of the external mixture. As a result, total Nccn are estimated for supersaturations of $s = 0.1\,\%$, $0.2\,\%$, $0.4\,\%$, $0.6\,\%$, $0.8\,\%$ and $1.0\,\%$, while species-related Nccn, which are sulfate (SU), sea salt (SS) as well as hydrophilic fractions of black carbon (BC) and organic matter (OM), are available for $0.2\,\%$ and $0.8\,\%$. Mineral dust aerosols are excluded entirely, following the argument that they do not contribute notably to Nccn as they are large in size and have a low hygroscopicity (Che et al., 2022). Not represented are aerosols related to volcanic eruptions, nitrate aerosols or stratospheric aerosols (Block et al., 2024). Currently, the publicly available dataset contains daily Nccn from 01/2003 to 12/2024 on a $0.75\,^\circ \times 0.75\,^\circ$ grid with 60 hybrid sigma-pressure levels from surface to top of atmosphere (Block, 2023). In the scope of the present study, only the years 2003 to 2021 have been used.

2.2 Observational data

The ground-based data that is used in this study to validate CAMS Nccn is provided by 25 measurement sites (Fig. 1). These stations were chosen because they measure Nccn for at least 4 different supersaturations. The full station names, the provided time periods and available supersaturations are listed in Tab. 1. References to all observational datasets are included in the Appendix, Tab. A1.

7 of these 25 stations are part of the European Aerosols, Clouds, and Trace gases Research InfraStructure (ACTRIS, http://www.actris.eu/): Cabauw (CES), Finokalia (FIK), Jungfraujoch (JFJ), Melpitz (MEL), Mace Head (MHD), Hyytiälä (SMR)

https://doi.org/10.5194/egusphere-2026-1404
Preprint. Discussion started: 30 March 2026

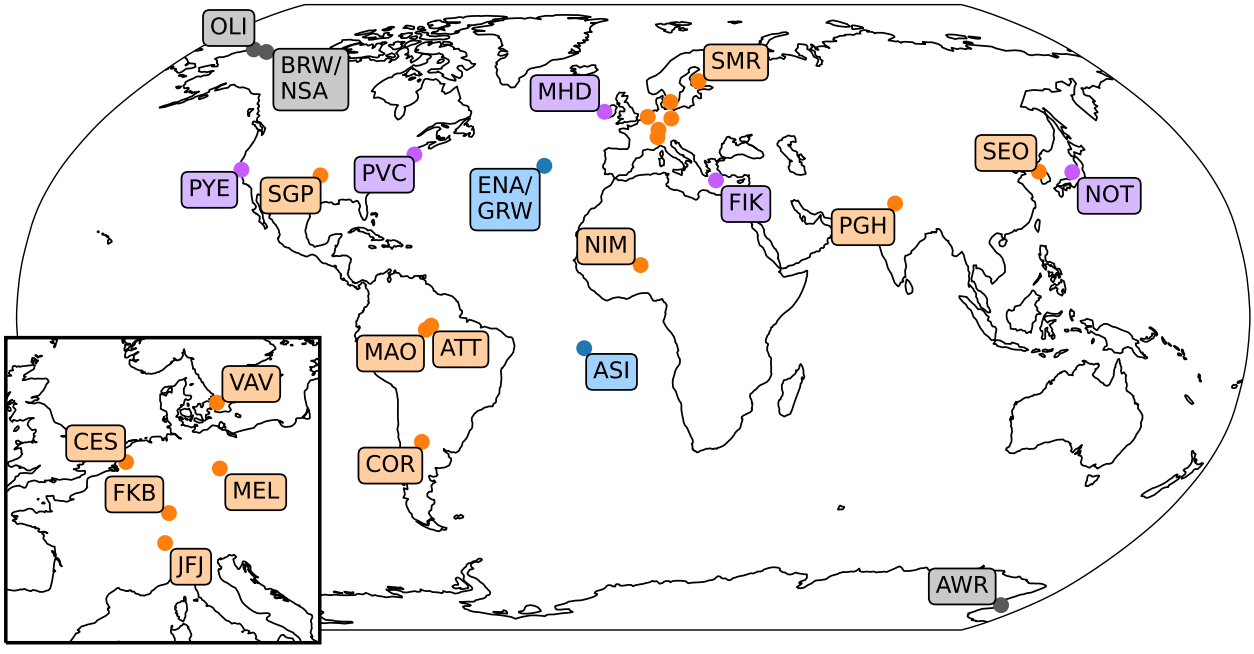

Figure 1. Locations of ground-based measurement sites. BRW and NSA as well as ENA and GRW share the same location, respectively. Continental stations in orange, remote marine in blue, coastal in purple and polar stations in grey. The full station names, provided time periods and available supersaturations of each measurement site are listed in Tab. 1.

and Vavihill (VAV). Information about these stations as well as about the stations of Seoul (SEO) in South Korea, Noto (NOT) in Japan, Utqiaġvik (formerly Barrow, BRW) in USA and Amazon Tall Tower Observatory (ATT; Pöhlker et al., 2016) in Brazil are given in Schmale et al. (2017, 2018). At each of these 11 stations, a single-column CCN counter (model CCN-100) by Droplet Measurement Technologies (DMT; Roberts and Nenes, 2005; Rose et al., 2008) was used.

The remaining 14 datasets from Ascension Island (ASI), McMurdo Station (Antarctica, AWR), Córdoba (COR), Graciosa Island (ENA and GRW, covering two time periods), Black Forest (FKB), Manacapuru (MAO), Niamey (NIM), North Slope of Alaska (NSA, same location as BRW), Oliktok Point (OLI), Nainital (PGH), Cape Cod (PVC), Point Reyes (PYE) and Southern Great Plains (SGP) are provided by the United States' Department of Energy's Atmospheric Radiation Measurement (ARM, https://www.arm.gov) user facility. Either single- or dual-column DMT CCN counters have been running at the ARM measurement sites and various data products were available at the time of this analysis. With the different data products, also varying levels of data quality checks were provided. The published data quality reports for each station (also see https://www.arm.gov/data/data-quality-program) have been used to remove suspect, incorrect and missing data. Furthermore, the following criteria have been applied to all datasets in the process of data checking: There must not be more than one single file per day of measurement. This file has to contain a valid time dimension and no negative Nccn or supersaturation values. A list

https://doi.org/10.5194/egusphere-2026-1404
Preprint. Discussion started: 30 March 2026

Table 1. Information on ground-based measurement sites that are used in this study. The given time frame indicates year and month of the first and last data point of the respective dataset of observations. The table contains a list of the supersaturations that are present in the given data files of each observation. For ARM stations, supersaturation setpoints are given. For SGP, four lists of supersaturations are provided, one for each available data product (AOSCCN, AOSCCNAVG, AOSCCN1COLAVG, AOSCCN2COLAAVG).

ID	Station name	Time frame	Available supersaturations [%]
ASI	Ascension Island (UK Overseas)	2016-04 - 2017-10	0.10, 0.20, 0.40, 0.60, 0.80, 1.00
ATT	Amazon Tall Tower Observatory, Brazil	2014-03 - 2015-02	0.11, 0.15, 0.20, 0.24, 0.29, 0.47, 0.61, 0.74, 0.92, 1.10
AWR	McMurdo Station, Antarctica	2016-05 - 2016-12	0.10, 0.20, 0.27, 0.37, 0.50, 0.61, 0.80, 0.92, 1.00
BRW	Utqiaġvik (formerly Barrow), Alaska US	2007-07 - 2008-06	0.20, 0.30, 0.50, 0.60, 1.00, 1.20, 1.45
CES	Cabauw, Netherlands	2012-01 - 2014-12	0.10, 0.20, 0.30, 0.50, 1.00
COR	Córdoba, Argentina	2018-09 - 2019-04	0.10, 0.20, 0.40, 0.60, 0.80, 1.00
ENA	Graciosa Island, Azores (Portugal)	2015-01 - 2020-10	0.10, 0.20, 0.50, 0.80, 1.00
FIK	Finokalia, Greece	2014-01 - 2015-12	0.20, 0.40, 0.60, 0.80, 1.00
FKB	Black Forest, Germany	2007-03 - 2008-01	0.08, 0.20, 0.34, 0.49, 0.78, 1.07, 1.37
GRW	Graciosa Island, Azores (Portugal)	2009-05 - 2010-12	0.10, 0.33, 0.55, 0.78, 1.00, 1.12
JFJ	Jungfraujoch, Switzerland	2012-01 - 2014-12	0.10, 0.15, 0.20, 0.25, 0.30, 0.35, 0.40, 0.50, 0.70, 1.00
MAO	Manacapuru, Brazil	2014-07 - 2014-09	0.15, 0.25, 0.40, 0.60, 0.80, 1.10
MEL	Melpitz, Germany	2012-01 - 2014-12	0.10, 0.20, 0.30, 0.50, 0.70
MHD	Mace Head, Ireland	2011-01 - 2012-12	0.10, 0.25, 0.35, 0.50, 0.75, 1.00
NIM	Niamey, Niger	2005-12 - 2007-01	0.20, 0.40, 0.60, 0.80, 1.00
NOT	Noto, Japan	2014-05 - 2015-03	0.10, 0.20, 0.50, 0.80
NSA	Northern Slope of Alaska, US	2007-03 - 2011-08	0.10, 0.23, 0.40, 0.56, 0.89, 1.23, 1.56
OLI	Oliktok Point, Alaska (US)	2017-04 - 2019-09	0.10, 0.20, 0.40, 0.60, 0.80, 1.00
PGH	Nainital, Uttarakhand (India)	2011-06 - 2012-03	0.06, 0.17, 0.31, 0.46, 0.60, 0.75
PVC	Cape Cod, Massachusetts (US)	2012-07 - 2013-03	0.15, 0.18, 0.22, 0.29, 0.36, 0.46, 0.55, 0.66, 0.74, 0.86, 0.94, 1.00
PYE	Point Reyes, California (US)	2005-03 - 2005-09	0.30, 0.50, 0.70, 0.90
SEO	Seoul, South Korea	2006-01 - 2010-12	0.20, 0.40, 0.60, 0.80
SGP	Southern Great Plains, Oklahoma (US)	2006-09 - 2021-12	0.15, 0.20, 0.40, 0.60, 0.80, 1.00, 1.15; 0.22, 0.27, 0.48, 0.68, 0.89, 1.10, 1.25; 0.00, 0.10, 0.20, 0.40, 0.80, 1.00; 0.08, 0.19, 0.34, 0.49, 0.79, 1.08, 1.38
SMR	Hyytiälä (SMEAR II), Finland	2012-01 - 2014-12	0.10, 0.20, 0.30, 0.50, 1.00
VAV	Vavihill, Sweden	2012-12 - 2014-11	0.10, 0.15, 0.20, 0.25, 0.30, 0.35, 0.40, 0.50, 0.70, 1.00, 1.40

https://doi.org/10.5194/egusphere-2026-1404
Preprint. Discussion started: 30 March 2026

of all removed dates is given in Tab. A1 in the Appendix. The measurements from ENA and GRW (Graciosa Island), as well as those from BRW and NSA (north of Alaska), were taken at the same ARM facilities.

At SGP, four different data products are available for overlapping time periods (Fig. A1), which we combined to one time series. Between two data products, which are available for the same period, we have always selected that one with the higher reported level of data quality. Thus, the AOSCCN (Aerosol Observing System Cloud Condensation Nuclei) product covers the period from 2006-09-13 to 2010-12-31, AOSCCNAVG (AOSCCN Average) from 2011-01-01 to 2012-10-31, AOSCCN1COLAVG (AOSCCN Single Column Average) from 2012-11-01 to 2017-08-16 and AOSCCN2COLAAVG (AOSCCN Dual Column Average) from 2017-08-17 to 2021-12-31.

Following Spracklen et al. (2011) who assessed an uncertainty range in observed Nccn of 5 to 40 % depending on the magnitude of concentrations, supersaturation and the type of CCN instrument used, we assume a maximum relative uncertainty of $\pm 40\,\%$ and a minimum absolute uncertainty of $\pm 20\,\mathrm{cm}^{-3}$ in observed Nccn, as was done in Block et al. (2024).

2.3 Data treatment

Please note that in the remainder of this study, $\mathrm{CCN_C}$ refer to Nccn derived from CAMS and $\mathrm{CCN_O}$ are observed Nccn. Supersaturation is abbreviated as s. In order to validate $\mathrm{CCN_C}$ with observed data, we processed and homogenized both datasets. The model height level is chosen such that the geopotential height of the nearest grid point to the measurement site matches the measurement altitude approximately. To reduce representativeness errors associated with comparing point-based observations to gridded model output, a horizontal mean of the nine nearest CAMS grid points surrounding each measurement site was used. This spatial averaging mitigates the influence of sub-grid variability and small spatial displacement errors. Using only the nearest grid point resulted in systematically lower correlation coefficients (not shown).

As a last step of preparation, for some stations the CAMS-derived Nccn are normalized from ambient temperature and pressure (ATP) to standard temperature and pressure (STP). This is done by using the ideal gas law for standard conditions ($T_0 = 273.15\,\mathrm{K}$, $p_0 = 1013\,\mathrm{hPa}$), as e.g., in Holanda et al. (2020) and Andrews et al. (2025):

$$\mathrm{Nccn_{STP}} = \mathrm{Nccn_{ATP}} \left(\frac{T_0}{T} \frac{p}{p_0} \right) . \tag{1}$$

Observational data of BRW, CES, FIK, JFJ, MEL, MHD, NOT, SEO, SMR and VAV are already given for STP conditions, while ATT data is normalized to STP using Eq. 1. Observed Nccn from ASI, AWR, COR, ENA, FKB, GRW, MAO, NIM, NSA, OLI, PGH, PVC, PYE, SGP are given for ATP conditions. Accordingly, CAMS-derived Nccn are compared to observations under the same conditions.

As mentioned, $\mathrm{CCN_C}$ are given at 6 specific supersaturations ($s = 0.1\,\%$, $0.2\,\%$, $0.4\,\%$, $0.6\,\%$, $0.8\,\%$ and $1.0\,\%$). Observed Nccn are usually not measured at the same supersaturations. Therefore, $\mathrm{CCN_O}$ are directly taken (or averaged if several exist) within a range of $\pm 0.05\,\%$. In case there is no data in the $\pm 0.05\,\%$ range, we interpolated linearly in the range of $\pm 0.1\,\%$. Since CAMS-derived Nccn are available only once per day (0 UTC), the hourly measured Nccn are averaged over each measurement day with the daily mean and standard deviation being computed.

https://doi.org/10.5194/egusphere-2026-1404
Preprint. Discussion started: 30 March 2026

In the files from the ARM sites, two types of supersaturations are given: One setpoint supersaturation and one calculated supersaturation, which can differ significantly, as described in Andrews et al. (2025) and Lance et al. (2006). Here, the calculated supersaturation was chosen as it resembles the actual supersaturation in the flow chamber. However, not all supersaturations are covered at each measurement site. A Nccn value that is missing at a supersaturation s_x, but available at s_1 and s_2, is estimated by applying a power law to a given Nccn value at $s_i \in [s_1, s_2]$:

$$\mathrm{Nccn}\,(s_x) = \mathrm{Nccn}\,(s_i)\left(\frac{s_x}{s_i}\right)^k , \tag{2}$$

with the exponent k given from:

$$k = \frac{\ln\left(\frac{\mathrm{Nccn}\,(s_1)}{\mathrm{Nccn}\,(s_2)}\right)}{\ln\left(\frac{s_1}{s_2}\right)} , \tag{3}$$

as it was derived e.g., in Block et al. (2024) and Désalmand (1985).

We limit the inter-/extrapolation interval $[s_1, s_2]$ to a maximum range of $\pm 0.4\,\%$ around the desired value s_x, to reduce the inaccuracies, which are introduced by using a constant slope k across a range of supersaturations.

Eq. 2 is a generalized form of the power law proposed by Twomey (1959), which has been widely used for the approximation of CCN activation spectra (e.g, Martins et al., 2009; Andreae, 2009; Hudson, 1980; Cohard et al., 1998). Commonly, s_i is assumed to be $1.0\,\%$ and the power law is written as

$$\mathrm{Nccn}\,(s_x) = \mathrm{Nccn}\,(1\,\%)s_x^k , \tag{4}$$

with a constant slope parameter k, that is independent of the desired supersaturation s_x.

2.4 Limitations to Twomey's power law

Several experimental and theoretical studies have pointed out that the simplicity of Twomey's power law comes with its limitations (e.g., Pöhlker et al., 2016; Deng et al., 2013; Ji and Shaw, 1998; Khvorostyanov and Curry, 2006; Cohard et al., 1998). Most importantly, it does not account for an aerosol-limited regime (e.g., Reutter et al., 2009) at high supersaturations, potentially leading to overestimated Nccn at high supersaturations. One reason is that the slope parameter k in Eq. 4 is assumed to be constant over the entire range of supersaturations, an assumption that has been contradicted by multiple observational studies (e.g., Kim et al., 2011; Khvorostyanov and Curry, 2006; Yum and Hudson, 2001). Instead, k has been shown to decrease with increasing supersaturation (Khvorostyanov and Curry, 2006; Cohard et al., 1998). The curvature of the activation spectrum depends on the size distribution of aerosol particles and thus, the environment of the respective air mass. Marine air masses with hygroscopic and bigger aerosol tend to have lower k values than continental environments, where small, hydrophobic particles are present (Jayachandran et al., 2020; Pruppacher and Klett, 1997). Cohard et al. (1998) stated that a power law with a constant k is not able to reproduce this curvature.

Several studies attempted to expand the original power law, e.g., using logarithmic (Wang et al., 2021) or exponential fits (Ji and Shaw, 1998). Khvorostyanov and Curry (1999) proposed a superposition of single-k power laws for different ranges of supersaturation and aerosol sizes, letting k decrease with increasing supersaturation and decreasing aerosol size.

https://doi.org/10.5194/egusphere-2026-1404
Preprint. Discussion started: 30 March 2026

In the following, we will show that using generalized s-dependent k parameters retrieved from observations give a very accurate representation of measured CCN spectra (Section 3.2) and are suited to be applied to simulated Nccn at one single supersaturation in order to create a full CCN spectrum.

2.5 Statistical approaches and analyzed parameters

The correlation between simulated and observed Nccn, as well as the quality of fit, have been assessed using the bias B, the Pearson correlation coefficient R and, as a combined metric, the Kling-Gupta efficiency (KGE).

The relative bias B is computed from the medians of CAMS-derived and observed Nccn:

$$B = \frac{\mathrm{med}\,(\mathrm{CCN_C}) - \mathrm{med}\,(\mathrm{CCN_O})}{\mathrm{med}\,(\mathrm{CCN_O})} \cdot 100\,\% \,. \tag{5}$$

A bias B of 0 corresponds to equal medians. Unless stated otherwise, the sign of the bias is kept and indicates overestimation (+) or underestimation (−). This means especially that an increasing B is not necessarily equal to a larger deviation of simulated to observed Nccn. It might as well indicate a transition from under- to overestimation. When averaging biases from a group of stations, the sign will be disregarded, which gives the absolute value $|B|$.

Following its standard definition, the Pearson R is

$$R = \frac{\sum_{i=1}^{n}(\mathrm{CCN_{O,i}} - \overline{\mathrm{CCN}}_\mathrm{O})(\mathrm{CCN_{C,i}} - \overline{\mathrm{CCN}}_\mathrm{C})}{\sqrt{\sum_{i=1}^{n}(\mathrm{CCN_{O,i}} - \overline{\mathrm{CCN}}_\mathrm{O})^2 \sum_{i=1}^{n}(\mathrm{CCN_{C,i}} - \overline{\mathrm{CCN}}_\mathrm{C})^2}} \,, \tag{6}$$

with n being the number of points in the observation period.

The Kling-Gupta efficiency (KGE; Gupta et al., 2009) is a metric used to quantify the quality of a model's fit to observations and is widely used in hydrology. It is employed here to jointly account for bias (quantified by B) and explained variability (represented by R) and is defined as

$$\mathrm{KGE} = 1 - \sqrt{(R-1)^2 + (\alpha-1)^2 + (\beta-1)^2} \,. \tag{7}$$

R is the Pearson correlation coefficient, $\alpha = \frac{\mathrm{std_C}}{\mathrm{std_O}}$ is the ratio of the standard deviations of $\mathrm{CCN_C}$ and $\mathrm{CCN_O}$, $\beta = \frac{\overline{\mathrm{CCN}}_\mathrm{C}}{\overline{\mathrm{CCN}}_\mathrm{O}}$ is the ratio of the means of $\mathrm{CCN_C}$ and $\mathrm{CCN_O}$. The higher a KGE value is, the better the fit is between observation and simulation. A maximum KGE of 1 is obtained for two perfectly matching datasets. Negative KGEs are possible but do not necessarily correspond to anti-correlating data or a certain sign of the bias. In this study, the KGE of each station is mainly used as a comparison metric and will always be related to other stations. An absolute statement, whether a certain number is considered high or low, will not be made.

Total median Nccn have been examined using the introduced metrics B, R and KGE. These primary metrics are further distinguished for their spatial variability (e.g., accounting for environmental setting and pollution regime) and for their variability in time (e.g., accounting for seasonal differences).

The assessed spatial variability is based on a classification defining the environment at each station as either remote marine, coastal or continental. Sites that are located south of 70° S or north of 70° N (outside the CAMS assimilation range) are classified as a separate group of polar stations.

https://doi.org/10.5194/egusphere-2026-1404
Preprint. Discussion started: 30 March 2026

Commonly, aerosol and CCN concentrations are also distinguished for different regimes. For example, Varghese et al. (2016) used a classification into clean (< 1000 cm^{-3}), polluted and highly polluted (> 2000 cm^{-3}), based on the Nccn at a supersaturation of 1 %. Andreae (2009) proposed a threshold of 600 cm^{-3} at 0.4 % supersaturation for polluted marine regions and Hudson and Yum (2002) defined groups of clean (< 200 cm^{-3}) and polluted air masses (> 1000 cm^{-3}) for 1 % supersaturation, with a transition regime in between. In this study, most analyses are based on 0.4 % supersaturation as a mid-range supersaturation level. At this supersaturation, a classification into a clean (CCN_O < 500 cm^{-3}), transient (500 cm^{-3} $\leq$ CCN_O < 800 cm^{-3}) and polluted (800 cm^{-3} $\leq$ CCN_O) regime has been constructed, which is similar to the mentioned classifications by Andreae (2009) and Hudson and Yum (2002), but with lower thresholds than in Varghese et al. (2016).

Since one aim of this study is to validate the spectral behavior of CAMS-derived Nccn, the sensitivity of the Nccn to a change in supersaturation will be used as a secondary metric. These Nccn-s spectra are approximated by applying Twomey's power law. The slope of the spectrum is then described by the slope parameter k, using Equation 3 for $s_1 = 0.1\,\%$ and $s_2 = 1.0\,\%$. The larger k the steeper the activation spectrum is. Large k are usually found for continental or polluted air masses (Martins et al., 2009; Pruppacher and Klett, 1997).

3 Results and discussion

3.1 The performance in time and space

Different environments and regimes certainly affect the order of magnitude of Nccn and thus the validity of CCN_C presented here. In order to compare different stations with each other we make use of the primary statistical quantities B, R and KGE from daily data and distinguish the stations by observed pollution regime and environmental setting. A summary is given in Tab. 2.

3.1.1 Evaluating the performance in time

Using the advantage of the CAMS-derived Nccn dataset as a continuous multi-year time series, a qualitative assessment of temporal presentability is made. Table 2 compares R values for each station distinguishing daily means, running means with windows of 11 days andcorrelations using monthly medians.

Using daily means, only 11 from 25 stations show R values above 0.5 indicating at least moderate correlation of the day-to-day fluctuations. To account for a full daily variability, it might be better if the full temporal frequency of 3-hourly CAMS reanalysis data would be used instead to derive Nccn. However, in the current dataset by Block (2023), this temporal resolution is not available due to limitations of computational resources and file storage.

Applying an 11-day running mean largely removes synoptic-scale variability, thereby improving temporal clarity of the time series at most stations. This filtering increases confidence that the CAMS-derived Nccn captures variability on synoptic time scales. Fig. 2 shows multi-year 11-day running medians of Nccn ($s = 0.4\,\%$) for all stations. Disregarding potential systematic

https://doi.org/10.5194/egusphere-2026-1404
Preprint. Discussion started: 30 March 2026

Table 2. Regime, environment, Kling-Gupta efficiency KGE, bias B, correlation coefficients R from daily averages, 11-day running means and monthly medians as well as number of days # for all 25 stations at s = 0.4 %, sorted by KGE from highest to lowest. R values in parentheses indicate not significant correlations (95 % confidence interval).

ID	regime	environment	KGE	B [%]	daily R	11-day R	monthly R	#
MHD	clean	coastal	0.667	+ 12.25	0.858	0.923	0.700	190
ATT	transient	continental	0.550	+ 12.26	0.723	0.868	0.837	224
SMR	transient	continental	0.398	− 40.99	0.589	0.786	0.935	814
CES	polluted	continental	0.361	− 37.59	0.617	0.645	0.723	565
VAV	transient	continental	0.335	− 28.40	0.452	0.322	0.707	395
FKB	polluted	continental	0.286	+ 26.05	0.590	0.710	0.808	278
NOT	polluted	coastal	0.272	− 17.41	0.310	0.605	0.831	258
PVC	transient	coastal	0.186	− 16.85	0.296	(0.098)	(0.360)	149
JFJ	clean	continental	0.166	− 51.72	0.646	0.739	0.955	594
ASI	clean	remote marine	0.094	+ 61.40	0.840	0.895	0.683	430
FIK	polluted	coastal	0.077	− 18.23	0.243	0.418	0.856	279
ENA	clean	remote marine	0.057	+ 31.76	0.187	0.278	0.649	706
MEL	polluted	continental	0.035	− 47.60	0.354	0.344	(0.166)	476
OLI	clean	polar	0.000	+ 141.39	(0.052)	(− 0.020)	(− 0.444)	234
SGP	polluted	continental	− 0.005	− 41.90	0.069	0.133	0.709	3873
NIM	transient	continental	− 0.017	+ 76.65	0.187	0.171	(0.401)	269
PGH	polluted	continental	− 0.031	+ 23.61	0.532	0.623	(0.480)	262
AWR	clean	polar	− 0.123	+ 215.42	0.612	0.836	0.910	210
GRW	clean	remote marine	− 0.210	+ 17.90	0.144	(− 0.034)	(0.077)	514
SEO	polluted	continental	− 0.262	+ 69.68	0.507	0.530	(0.570)	634
COR	transient	continental	− 0.286	− 65.53	(− 0.115)	(− 0.095)	(− 0.537)	192
NSA	clean	polar	− 0.408	− 42.89	0.164	0.240	(0.025)	1395
PYE	clean	coastal	− 0.426	+ 84.65	0.244	(0.047)	(− 0.213)	186
MAO	polluted	continental	− 0.585	+ 77.09	0.628	0.713	(− 1.000)	41
BRW	clean	polar	− 2.383	− 16.61	(0.079)	0.171	(0.097)	167

offsets at this stage, the simulated temporal variability agrees well with the observations for the majority of stations. A more detailed analysis on short-term variability of selected sites is given in Anders et al. (2025).

Correlating monthly median Nccn (Fig. A2), the correlation coefficients increase again for 10 stations compared to their 11-day R values, especially for VAV, FIK, ENA and SGP the increase is quite drastic. With in total 13 out of 25 stations showing significant R values above 0.5, we conclude that CAMS-derived Nccn reproduce the observed variability very well on seasonal and annual time scales and therefore is very suitable to be used as a climatology.

https://doi.org/10.5194/egusphere-2026-1404
Preprint. Discussion started: 30 March 2026

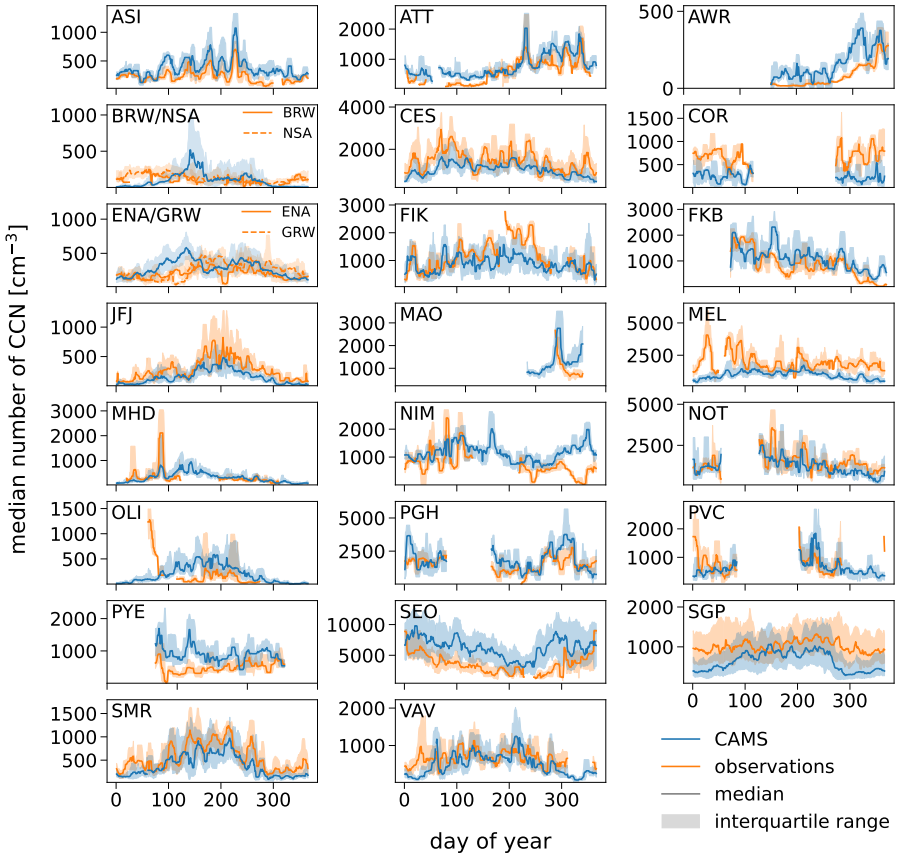

Figure 2. Climatologies for all stations at a supersaturation of 0.4 %. CCN_C in blue and CCN_O in orange, both with a running median and interquartile range in a window of 11 days. Please note: Data from 29 February has been removed and the co-located data from BRW and NSA as well as ENA and GRW are shown in the same tile.

Further analysis on the seasonality reveals that CAMS is generally very capable to reproduce seasonal cycles of Nccn, as was already depicted in Block et al. (2024). At stations featuring wet and dry seasons, such as ATT, FIK and SEO (Pöhlker et al., 2016; Kouvarakis et al., 2000; Schmale et al., 2018), the increase in observed dry season Nccn is well captured by CAMS-derived Nccn (not shown).

3.1.2 Dependencies on environment and pollution regime

Systematic differences in KGE at one fixed supersaturation (here 0.4 %), when comparing the three environments, can not be found. Averaging between all remote marine stations results in a KGE of -0.020, for coastal a KGE of 0.155 and for continental stations 0.073. These differences are small compared to the spread between stations of the same environment (Tab. 2). Furthermore, analyzing the KGE in dependence of the stations' geographical position or their pollution regime has given no clear result either.

https://doi.org/10.5194/egusphere-2026-1404
Preprint. Discussion started: 30 March 2026

However, neglecting the polar stations (which are unconstrained in CAMS), four out of five stations with the lowest KGE are in the polluted regime (MAO, PGH, PYE, SEO). These four stations exhibit a strongly positive B, meaning that their CCN_O are significantly overestimated. Similarly, Block et al. (2024) stated in their first validation of CAMS-derived Nccn that very polluted sites seem to be overestimated. The results of the present study coincide with their conclusion.

Most stations fall in the respective pollution regime category as defined by observations. Only 6 stations deviate as a result of their bias, and thus would fall into a different category. Due to their negative bias, SMR, VAV and COR would be clean regimes instead of transient ones and SGP would be transient instead of polluted. Meanwhile NIM would be polluted instead of transient and PYE would be polluted instead of clean due their positive bias. A decrease in bias would lead to a correction of pollution regime identification.

3.1.3 Polar sites

Four sites (AWR, BRW, NSA and OLI) lie in polar regions and therefore outside of the global domain of the data assimilation scheme of ECMWF's IFS between 70° S and 70° N. Due to possible irregularities caused by the lack of observational constraints in this area, CAMS-derived Nccn data need to be used carefully. In particular, the co-located stations BRW and NSA exhibit simulation features that did not appear at any other station. There are partially sharp peaks, exceeding the observations by a factor of up to 4, and extremely low concentrations below $1\,cm^{-3}$ in the winter months. These extremes result in very low correlation coefficients at both BRW and NSA. The same holds for the nearby station OLI. The Antarctic station AWR, however, exhibits a value of R that is comparable to stations of the mid-latitudes but it produces a very large bias (Tab. 2) even though, both CCN_O and CCN_C are very low. The presence of wrong peaks and large biases illustrates very clearly that the benefits of the assimilation of satellite observations are missing for the polar regions.

3.2 The CCN-supersaturation spectrum

3.2.1 Evaluating the CCN spectrum

As depicted from Fig. 2, CCN_O are overestimated at some stations (e.g., AWR, NIM or ASI), while underestimation is present at others (e.g., MEL, JFJ or SGP). These offsets change depending on the chosen supersaturation (Anders et al., 2025) as different fractions of CCN species get activated and thus shape the CCN spectrum.

Fig. 3 compares observed and CAMS-derived Nccn-supersaturation spectra, which are computed from median Nccn for all six supersaturations, for which CAMS-derived total CCN are available. Both, CCN_C and CCN_O increase with supersaturation as expected. However, while CCN_O show a shallower slope for higher supersaturations, CCN_C grow almost linear with supersaturation and do not reach an aerosol-limited regime as the observations. Consequently, this leads to both an overestimation (positive bias B) at high supersaturations and an underestimation for low supersaturations. For 22 out of 25 stations, B at a supersaturation of 1.0 % is larger (more positive or less negative) compared to its value at 0.1 % (Tab. A2). However, at 15 stations, the absolute value $|B|$ is larger at low supersaturations. In the median of all stations, the absolute value $|B|$ is 69.68 %

https://doi.org/10.5194/egusphere-2026-1404
Preprint. Discussion started: 30 March 2026

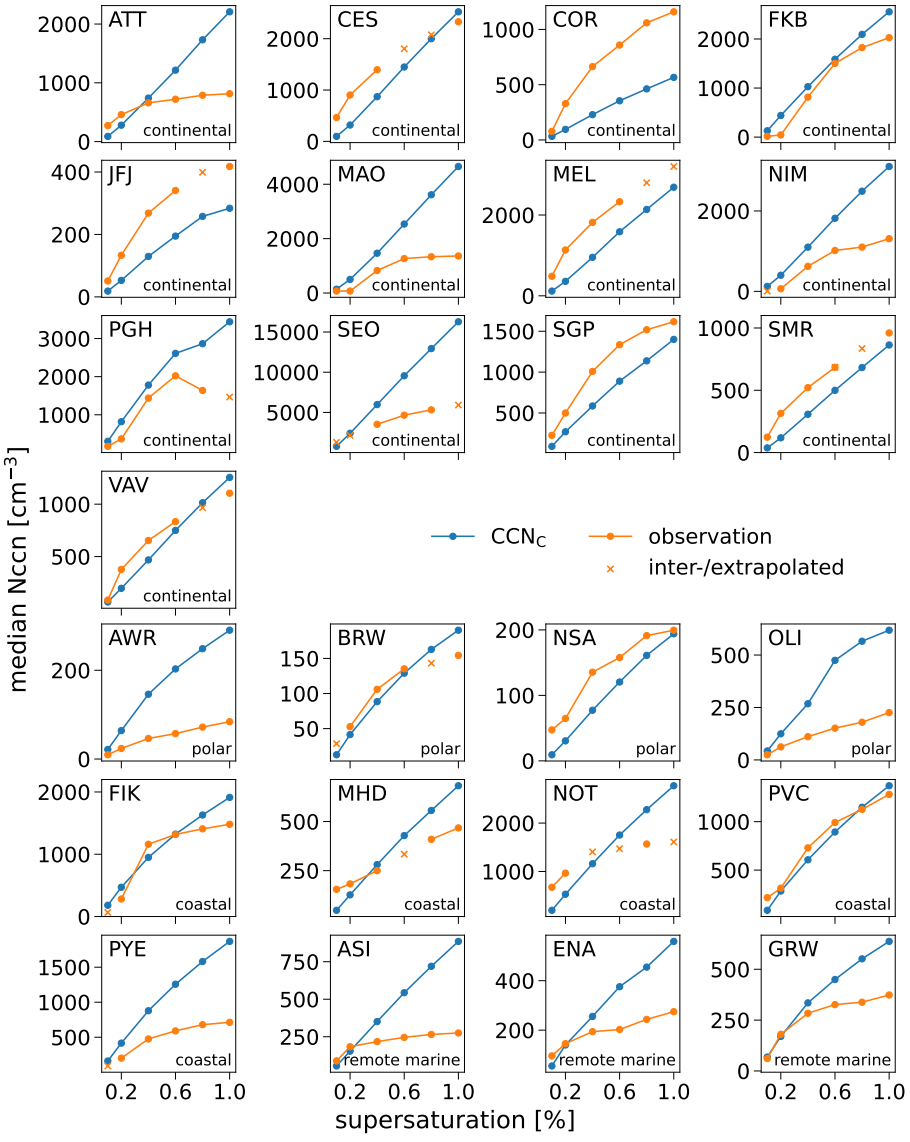

Figure 3. Nccn-s spectra showing the medians of every analyzed ground-based measurement campaign over the corresponding supersaturation. CCN_C in blue and CCN_O in orange. Observation values that are indicated by an 'x' are medians of an inter- or extrapolated set of daily Nccn, using Twomey's power law (Eq. 2). Please note, the y axis is different in every plot. The x axis is shared.

for s = 0.1 % and 51.16 % for s = 1.0 %. Hence, the underestimation at low supersaturations (which is reached more often in natural cloudy conditions) is an at least equally important issue as the overestimation at high supersaturations.

As found by Anders et al. (2025), the best-fitting supersaturation s_{best}, for which B is closest to zero, differs between stations. As depicted in Fig. 4 and listed in Tab. A2, remote marine stations are least biased at low supersaturations and thus

https://doi.org/10.5194/egusphere-2026-1404
Preprint. Discussion started: 30 March 2026

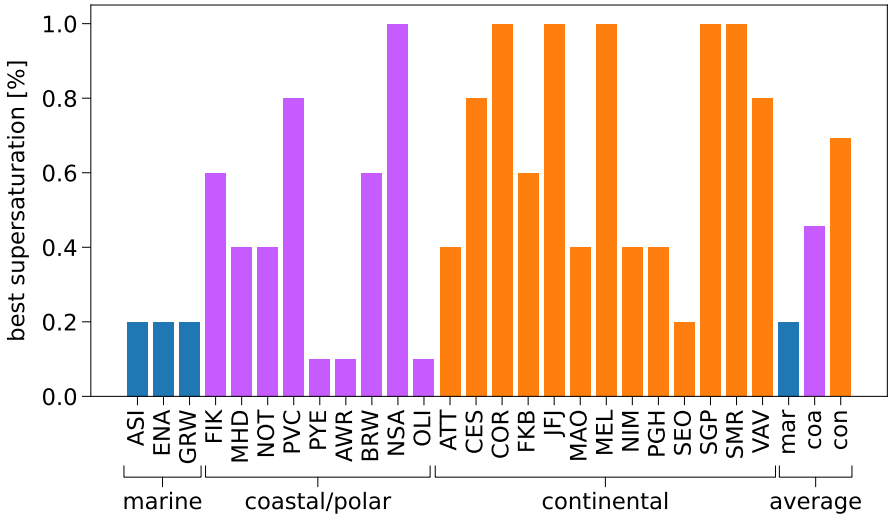

Figure 4. Supersaturation where CCN_C and CCN_O show best fit, for each station respectively. Distinguished into marine (blue), coastal/polar (purple) and continental (orange) environments, also showing the respective mean of each group.

obtain an s_{best} of around 0.2 %. Both, coastal and polar stations vary widely in bias within their respective categories and are therefore combined here. They receive an average s_{best} of around 0.4 % while continental stations show rather high s_{best} of around 0.6 %. It needs to be noted here, that we did not find any dependence of s_{best} on the pollution regime.

The curvature of the CCN spectrum and thus the bias for each supersaturation might be dependent on the involved aerosol species. As already depicted in Block et al. (2024), Nccn derived from CAMS are mostly dominated by organic matter (OM) and sulfate (SO4), while black carbon (BC) fractions are mostly small and the fractions of the three sea salt (SS) modes are negligible, even under remote marine conditions. With higher supersaturation, smaller and less hygroscopic aerosols get activated. Hence, the OM and BC fractions increase with supersaturation, while the portions of SO4 and SS are reduced. Looking at the ratio of the OM and SO4 fractions, we found a a very clear relationship to the above-mentioned slope parameter k (Fig. 5): The larger the OM-to-SO4 ratio, the larger is k. A logarithmic fit was found with an R^2 of 0.866. Large OM-to-SO4 ratios above 1.5 at 0.2 % supersaturation are found at MAO, NIM and ATT. These three stations indeed exhibit similar shapes in Fig. 3, having a strongly increasing B with increasing supersaturation. On the other hand, stations with low OM-to-SO4 ratios (FIK, AWR and BRW), below 0.3 at 0.2 % supersaturation, tend to have a weaker increase in B. It seems that the stations with lower OM fractions are likely to have a smaller absolute value $|B|$, but tend to produce a lower correlation coefficient R. As a result of these two contradictory effects, a systematic relation of the OM-to-SO4 ratio on the KGE could not be determined. Examining the sea salt and BC fractions, no significant correlation to the KGE is obtained either.

This specific feature suggests a possible cause of the biased CCN spectrum. The discrepancy could stem from uncertainties in the emission fractions of CCN-relevant aerosol species (as these are not constrained in CAMS), from limitations in the

https://doi.org/10.5194/egusphere-2026-1404
Preprint. Discussion started: 30 March 2026

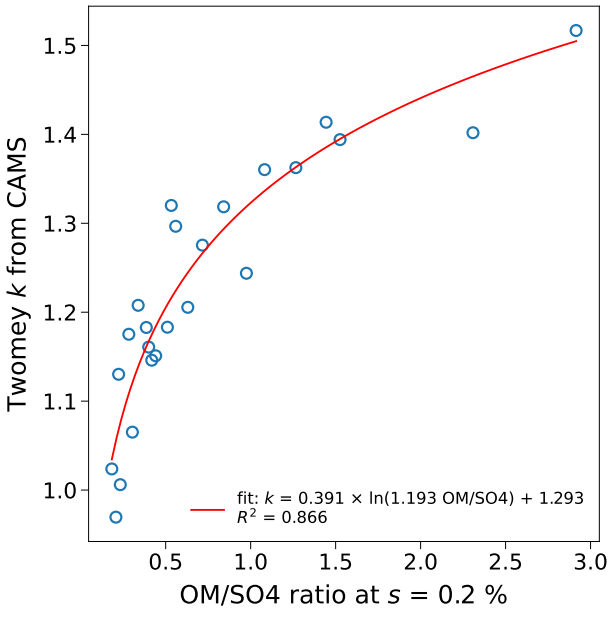

Figure 5. Slope parameter k from CCN_C, as defined by Equation 3 with $s_1 = 0.1\,\%$ and $s_2 = 1.0\,\%$, against the ratio of the median organic matter (OM) and sulfate (SO4) CCN_C fractions. Each data point (blue circle) represents one station. A logarithmic fit was performed (red solid line).

assumed aerosol size distributions and composition used in the CCN calculations (e.g., fixed global modes and kappa values, assumption of external mixtures), or from a combination of both. Nevertheless, the overall Nccn spectrum may be improved without modifying aerosol size distributions or species concentrations. Instead, this approach relies solely on the observed CCN spectrum as demonstrated in the following section.

3.2.2 Deriving a spectral $k(s)$ from observations

As described in the previous section, we found large biases in CAMS-derived Nccn at both low and high supersaturations. To reduce these biases, we present an approach tailored to the unique characteristics of the CAMS-derived Nccn dataset. The idea is to fit the simulated Nccn-s spectrum to the observations. For that, due to its simplicity and its prevalent application in CCN activation spectra (e.g., Martins et al., 2009; Cohard et al., 1998), we use Twomey's power law (Equation 4). However, its original form must be modified to serve the targeted purpose, reducing biases in CCN_C at both low and high s.

First of all, we can not use 1.0 % as the reference supersaturation s_i, since this would preserve the large biases at this supersaturation. Instead, we use an environment-specific reference, which accounts for the different s_{best} we found in the previous section for the different environments (Fig. 4). Based on these findings, we defined three environment-specific s_i: 0.2 % for remote marine, 0.4 % for coastal and polar sites and 0.6 % for continental environment.

https://doi.org/10.5194/egusphere-2026-1404
Preprint. Discussion started: 30 March 2026

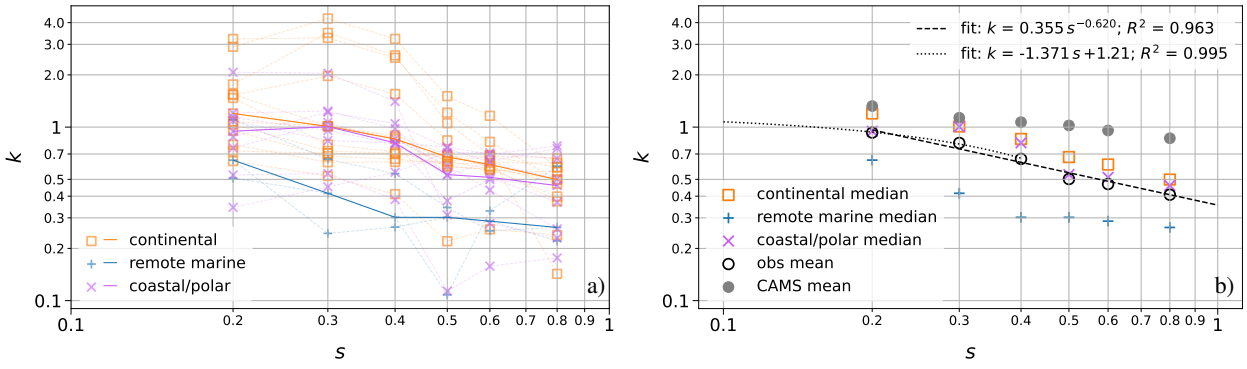

Figure 6. The power law exponent $k\,(s)$, derived from the observations (Eq. 3) and grouped by the environment. a) The $k\,(s)$ spectra of all 25 measurement sites. Continental stations are indicated by an orange square, remote marine medians by a blue '+' and coastal/polar stations by a purple 'x'. The medians of each environment are shown with solid lines in the respective color. b) Averaged and fitted observation-derived $k\,(s)$. The medians of each environment are shown by using the same markers as in a). The black empty circles mark the average between continental, marine and coastal/polar medians from the observations (obs mean). Grey filled circles represent the average between continental, marine and coastal/polar medians from CAMS-derived Nccn (CAMS mean). A power law fit (dashed line) has been applied to the observational mean. Additionally, a linear fit (dotted line) is used for the lower part of the supersaturation spectrum and has been derived from the points at $s \leq 0.4$. Please note, that PGH data points at 0.8 % and 1.0 % are excluded from both plots and the derivation, in order to prevent negative values of $k(s)$.

Generalizing Twomey's power law by applying it to other supersaturations than 1.0 % has been done already (e.g., Block et al., 2024; Andreae, 2009) and in our case, it is a promising modification to avoid high-supersaturation biases and to target each environment specifically. It needs to be noted that this flexibility in particular is the main advantage of the power law over other parametrizations. The exponential function by Ji and Shaw (1998), the error function by Pöhlker et al. (2016) and the logarithmic formulation by Wang et al. (2021) all have Nccn (1.0 %) as one of their inputs. We do not want to evaluate the capabilities of all these parametrizations for fitting observed Nccn-s spectra here as they are not suitable for our purpose.

Furthermore, we found for our data that keeping a constant exponent k in the power law leads to increased biases at low supersaturations. Similar results have been shown e.g., by Kim et al. (2011) and Wang et al. (2021). Furthermore, k derived from observations decrease with supersaturation (e.g., Khvorostyanov and Curry, 2006; Cohard et al., 1998; Yum and Hudson, 2001). This is also the case for the observations we use in this study: Fig. 6 a) depicts k values of each station, as calculated from Eq. 3. In marine environments, k is usually lower than over the continents (Jayachandran et al., 2020; Pruppacher and Klett, 1997).

We propose to use these observation-derived, spectral $k\,(s)$ instead of a constant k in the power law:

$$\mathrm{Nccn}\,(s_x) = \mathrm{Nccn}\,(s_i)\left(\frac{s_x}{s_i}\right)^{k\,(s)}. \tag{8}$$

https://doi.org/10.5194/egusphere-2026-1404
Preprint. Discussion started: 30 March 2026

Similar notations of a power law with a supersaturation-dependent exponent have been used by e.g., Khvorostyanov and Curry (2006), Khvorostyanov and Curry (2008) and Liu et al. (2011). For the purpose of reducing low supersaturation biases in CCN_C and ultimately, simulating a more accurate CCN activation spectrum, this approach is suitable to modify the yet too steep slope of the CCN_C spectrum.

As a first step, we average the obtained station-specific $k(s)$, to obtain a global spectrum. Since the majority of stations we use are continental, calculating the median across all stations would result in a bias towards the continental stations. Thus, we group the observation-derived $k(s)$ spectra of the stations in each environment, compute the median of each group (depicted as solid lines in Fig. 6 a) and finally, average these three medians for each supersaturation, to obtain a global spectrum of observation-derived $k(s)$ from equally weighted environments (Fig. 6 b). For comparison, we calculated the same global, equally environment-weighted mean $k(s)$ from CCN_C. It becomes clear that the observation-derived $k(s)$ (obs mean) differ widely from the CAMS-retrieved $k(s)$ (CAMS mean), revealing the root of the biased CAMS-derived CCN spectrum.

Lastly, to reduce the risk of overfitting to our set of observations and to extrapolate $k(s)$ to 0.1 % and 1.0 %, we applied a power law fit for supersaturations starting at 0.2 % and a linear fit extrapolating to 0.1 %. The power law appears to be the best-fitting function for the given points of $k(s)$ (obs mean). The second linear fit is necessary due to the nature of the power law, which would grow to infinity at low values of s. Similarly, Khvorostyanov and Curry (2006) have found observed k spectra to decrease more slowly in the range below 0.12 % supersaturations compared to higher s. Wang et al. (2021) used a piecewise function that fits Nccn below 0.1 % linearly, which gives better results than the Twomey parametrization.

Using ATT as an example, we compare some of the mentioned approaches in Fig. A3 and show how the CAMS CCN spectrum would behave for different approaches. All parametrizations are obtained by applying Equation 8 with $s_i = 0.6\,\%$, which is the reference supersaturation for the continental environment. As mentioned above, the major advantage of using an s-dependent $k(s)$ instead of a constant k is the ability to reduce low-s biases. The station-specific $k(s)$ is derived from the observations at ATT only and the environment-specific $k(s)$ is the median of all continental stations. Since the differences between environment-specific and global $k(s)$ are not very large, we decided to keep the global parametrization and not to distinguish between the environments, as we did for the definition of s_i. Please note that all 25 stations behave differently, which is why the chosen parametrization is not necessarily the best fit at each station. It is rather a tradeoff between the individual stations and has to be applicable on a global scale.

Finally, our $k(s)$ parametrization can be written as in Fig. 6 b:

$$k(s) = \left\{ \begin{array}{ll} -1.371028\,s + 1.210104 & \text{for } s < 0.2\,\% \\ 0.355152\,s^{-0.619866} & \text{for } s \geq 0.2\,\% \end{array} \right\} . \tag{9}$$

Applying Equation 9 to the six supersaturations CAMS-derived Nccn are available at, we receive a global spectrum of $k(s)$ values, which are independent of the environment.

https://doi.org/10.5194/egusphere-2026-1404
Preprint. Discussion started: 30 March 2026

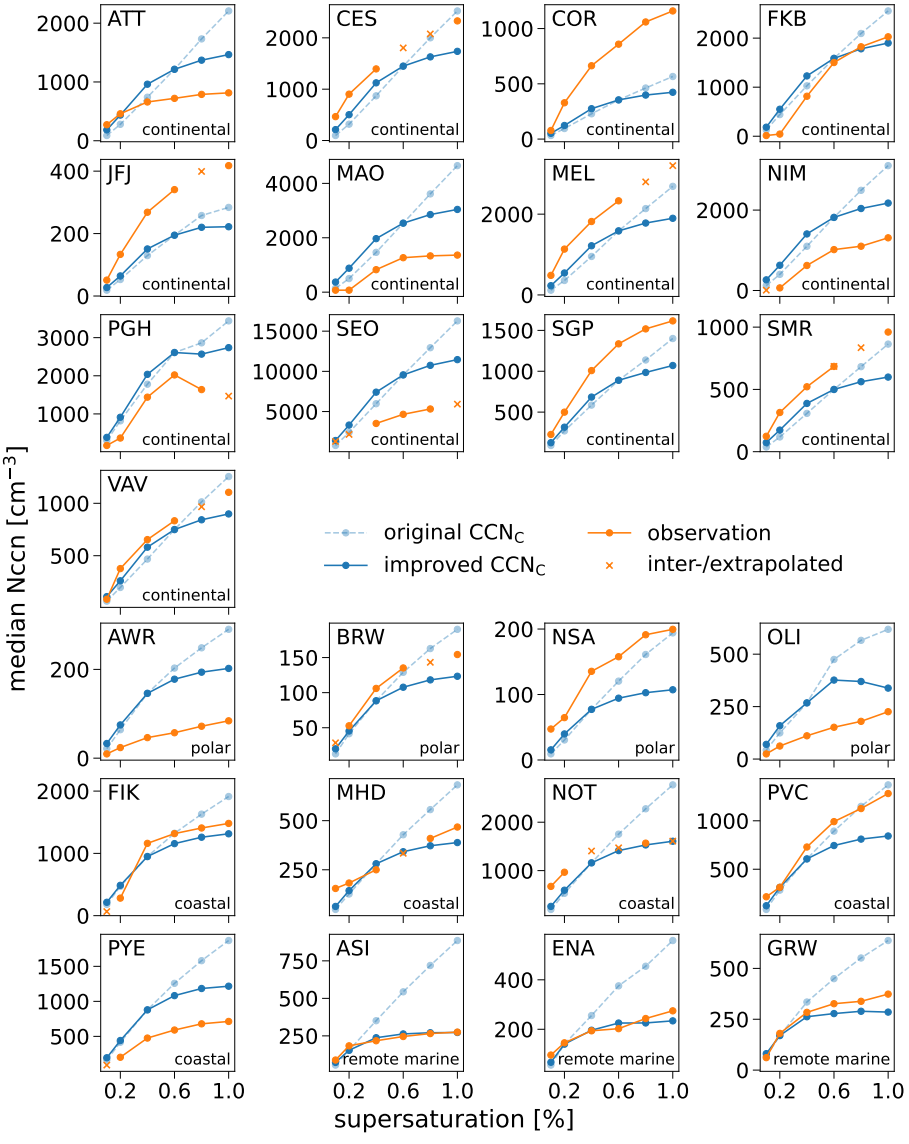

Figure 7. Same as Fig. 3, but with the addition of improved CCN_C (dark blue).

https://doi.org/10.5194/egusphere-2026-1404
Preprint. Discussion started: 30 March 2026

3.2.3 Towards an improved CCN spectrum

Using the new global set of s-dependent k values and the environment-specific s_i, we applied Equation 8 to the original daily $\mathrm{CCN_C}\,(s_i)$. The resulting medians are depicted in Fig. 7, which illustrates the improvement this new approach achieved. The curvature of the activation spectra at most stations is simulated more accurately. Especially, at the remote marine stations ASI, ENA and GRW as well as coastal FIK, MHD and NOT, this is the case. In addition, ATT, MAO, NIM and SEO are examples from the continental environment where high supersaturation biases are reduced significantly. However, Nccn which the original $\mathrm{CCN_C}$ have already underestimated (e.g., for CES, COR, JFJ, MEL, SGP, SMR) do not benefit from the adjustments and negative biases at continental stations and high supersaturations are enhanced. To account for these very region-specific biases, a modification of the underlying size distribution for CAMS-derived Nccn or a redistribution of CCN-relevant aerosol masses might still be necessary.

Despite these remaining challenges, we could reduce the biases for the majority of all stations (Fig. A4 in the appendix). Especially at the high supersaturations 0.8 % and 1.0 %, the absolute values of the bias are decreased substantially, improving the coastal, polar and remote marine stations. Also at low supersaturations, absolute biases $|B|$ are reduced in all environments. Specifically, the medians of the biases of all stations at 0.1 %, 0.2 %, 0.4 %, 0.6 %, 0.8 % and 1.0 % supersaturation are reduced by 24.3 %, 25.6 %, 19.4 %, 12.9 %, 22.5 % and 26.4 %, respectively. At 0.4 % and 0.6 %, the reduction rates are lowest, since these supersaturations have been used as reference points for the majority of the stations. The improved median absolute values $|B|$ are 52.8 %, 44.9 %, 33.0 %, 29.1 %, 35.1 %, 37.6 %, respectively. Unlike Fig. A4, these absolute values do not indicate a direction of the bias (under-/overestimation) but show that we could reduce the magnitude of the biases at all supersaturations substantially.

4 Summary and conclusions

The recently published 3D-dataset of CCN number concentrations (Nccn) derived from CAMS reanalysis aerosol mass mixing ratios (Block et al., 2024) is evaluated with direct observations from 25 ground-based measurement sites. Specific focus was put on the performance of CAMS-derived total Nccn in three categories: 1. its variability in time, ranging from short-term variability over seasons to climatologies, 2. its suitability in different environments (remote marine, coastal, continental and polar) and pollution regimes (clean, transient and polluted) and 3. its sensitivity to supersaturation.

Considering the variability in time, a wide spread, also within each environment or pollution regime, was found. Especially, the accuracy of the daily variability differs between all stations, with Pearson correlation coefficients ranging between -0.07 and $+0.86$. Since CAMS-derived Nccn are only available as snapshots at 0 UTC, the variability over the day is neglected and this is reflected in the poor results of daily correlation for most stations. Decreasing the temporal frequency used for correlation over time revealed increased performance. Significant correlation coefficients using monthly-means ranged between $+0.65$ and $+0.95$. Furthermore we found that CAMS-derived Nccn are able to reproduce climatological and seasonal variability, also representing dry and wet seasons, with good accuracy.

https://doi.org/10.5194/egusphere-2026-1404
Preprint. Discussion started: 30 March 2026

Considering the suitability of CAMS-derived Nccn in different environments and regimes, we made use of Kling-Gupta efficiency (KGE) as an estimate of quality of fit, taking into account correlation as well as bias. The resulting values show a large spread between stations and no clear dependence of the model's performance to environmental settings nor to pollution regimes. However, we did find that four out of five stations with the highest median CCN_C exhibit a positive bias larger than 20 %. This affirms the question of Block et al. (2024) whether there might be a tendency to overestimation at heavily polluted sites. Arctic and antarctic stations appeared to be problematic as well, as the data assimilation scheme is only active between 70° S and 70° N, possibly causing large biases and low correlation coefficients that have been obtained at some of the investigated polar stations. Thus, one should be careful when using the CAMS-derived CCN dataset in these regions.

The examination of the sensitivity of Nccn to different levels of supersaturation revealed an increasing bias with increasing supersaturations. At some stations, this implies a change from underestimation to overestimation when increasing the supersaturation. The bias shift could be described using the slope parameter k of Twomey's power law, which was applied onto the CCN-supersaturation spectrum. For almost all stations, CAMS-derived Nccn exhibit a larger k than observed Nccn, which is related to a too steep activation spectrum. This was found to be related to the OM-SO4 ratio of species CCN, hinting to potential causes in the emission fractions and/or underlying assumptions in the size distributions. Stations with a lower OM-to-SO4 ratio in the CCN species often obtain a lower k. Thus, modifying the underlying size distribution might bring CAMS-derived Nccn even closer to the observations. This approach was not pursued in this study but may be subject to further development of the dataset. Nevertheless, our improvements of CAMS-derived Nccn solely relying on observations already enhance the great potential of this CAMS CCN dataset for global aerosol-cloud-interaction studies.

A significant reduction of the biases in CAMS Nccn could be achieved by applying a modified power law with an s-dependent k spectrum, which has been derived from the observations. At a supersaturation of 1.0 %, the bias decreased in the median by 26.4 % to an absolute value of 37.6 %, indicating a reduction of the overestimation. For lower supersaturation of 0.1 %, it decreased by 24.3 %, to an absolute value of 52.8 %, which corresponds to a reduction of the underestimation at this supersaturation. The majority of stations exhibited more accurate presentations of their CCN-supersaturation spectra, especially those in remote marine or coastal environment. However, biases at high supersaturations persist at some stations.

Despite our efforts of exploring and evaluating CAMS-derived Nccn, further investigations should also focus on the validation of the vertical distribution, as some problems have already been addressed by Kulkarni et al. (2025). It is also of importance to investigate the quality of CAMS-derived Nccn in the southern hemisphere and above the Southern ocean, since this study could only partially contribute to the discussion started by Choudhury et al. (2025). Additionally, the comparison to more stations of long-term CCN measurements over multiple years will help in assessing the representation of not only day-to-day but also seasonal variability and eventually multi-decadal trends.

5 Data availability

The CAMS-derived CCN data (https://doi.org/10.26050/WDCC/QUAERERE_CCNCAMS_v1) from Block (2023) that is being evaluated here, is archived at the World Data Center for Climate (WDCC) at DKRZ and can be downloaded from

https://doi.org/10.5194/egusphere-2026-1404
Preprint. Discussion started: 30 March 2026

https://www.wdc-climate.de/ui/entry?acronym=QUAERERE_CCNCAMS_v1.

An overview of the 25 evaluation datasets can be found in Table 1 and Table A1, with references therein.

10 of the 25 CCN datasets providing CCN data at various supersaturations (Cabauw (CES), Finokalia (FIK), Jungfraujoch (JFJ), Melpitz (MEL), Mace Head (MHD), Hyytiälä (SMR), Vavihill (VAV), Utqiaġvik - formerly Barrow(BRW), Noto (NOT), Seoul (SEO)) were obtained from https://doi.org/10.6084/m9.figshare.c.3471585.v1 (Petäjä et al., 2017).

CCN data for 14 of our 25 stations (Ascension Island (ASI), McMurdo Station (Antarctica, AWR), Cordoba (COR), Graciosa Island (ENA and GRW, covering two time periods), Black Forest (FKB), Manacapuru (MAO), Niamey (NIM), North Slope of Alaska (NSA, same location as BRW), Oliktok Point (OLI), Nainital (PGH), Cape Cod (PVC), Point Reyes (PYE) and Southern Great Plains (SGP)) were provided by the United States' Department of Energy's Atmospheric Radiation Measurement (ARM, https://www.arm.gov) user facility.

The data for ATTO Observatory (ATT) was directly provided by Mira Pöhlker (Pöhlker et al., 2016). The Supplement related to this article is available online at https://doi.org/10.5194/acp-16-15709-2016-supplement.

https://doi.org/10.5194/egusphere-2026-1404
Preprint. Discussion started: 30 March 2026

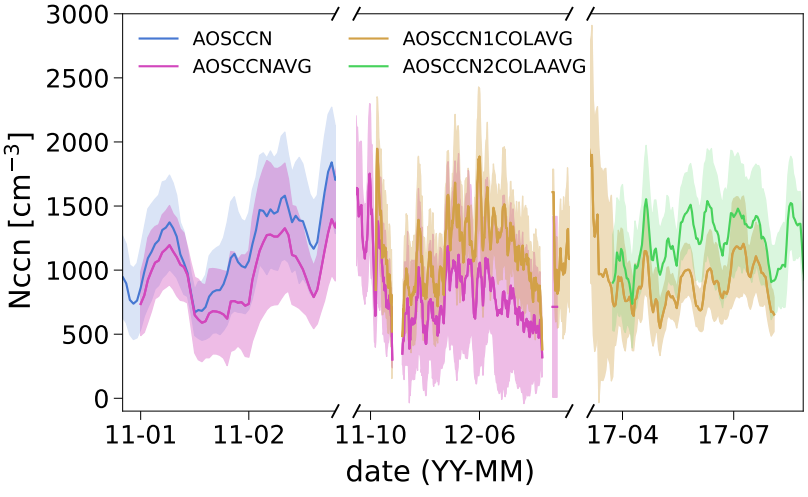

Figure A1. All four data products of SGP that have been combined to one time series, which we used in our analysis. Daily Nccn are given at 0.4 % supersaturation and with a 11-day running mean. The standard deviation of daily averaged observational data is represented by colored shading.

https://doi.org/10.5194/egusphere-2026-1404
Preprint. Discussion started: 30 March 2026

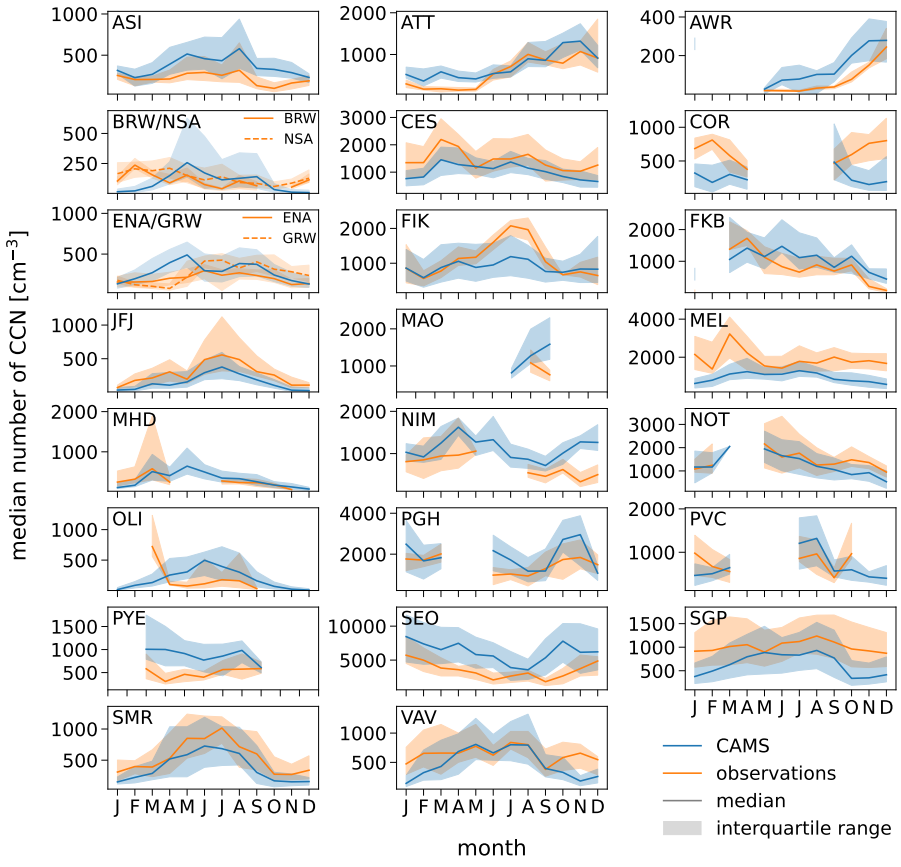

Figure A2. Climatologies for all stations at a supersaturation of 0.4 %. CCN_C in blue and CCN_O in orange, both showing monthly medians and interquartile ranges. Please note: The co-located data from BRW and NSA as well as ENA and GRW are shown in the same tile.

https://doi.org/10.5194/egusphere-2026-1404
Preprint. Discussion started: 30 March 2026

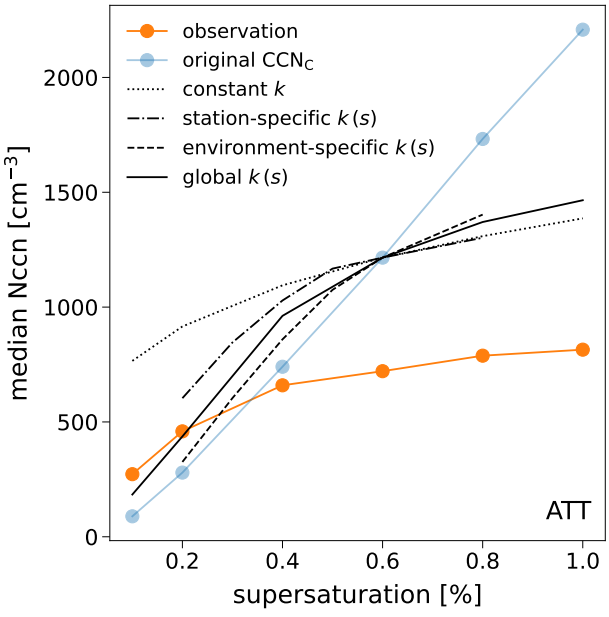

Figure A3. Nccn-s spectrum at ATT, showing the median Nccn over the corresponding supersaturation. Original CCN_C in blue, CCN_O in orange and four different parametrizations of CCN_C in black: The constant k is calculated from Eq. 3 with $s_1 = 0.4\,\%$ and $s_1 = 0.8\,\%$. The station-specific $k(s)$ is derived from the observations at ATT only and the environment-specific $k(s)$ is the median of all continental stations. The global $k(s)$ is the mean of the three environment medians. All four Nccn parametrizations are then retrieved from Eq. 8 with the respective $k(s)$ and a reference supersaturation s_i of $0.6\,\%$.

https://doi.org/10.5194/egusphere-2026-1404
Preprint. Discussion started: 30 March 2026

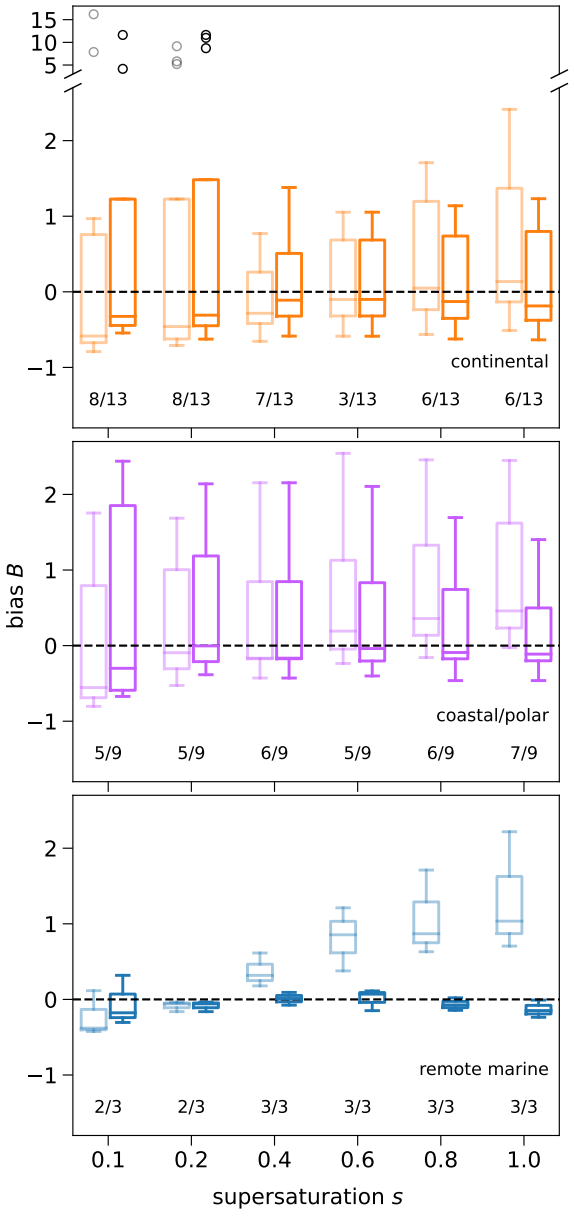

Figure A4. Statistics of the bias B at each supersaturation, depicted for continental (orange), coastal/polar (purple) and remote marine environment (blue). CAMS-derived Nccn in light hue and the improved new CCN_C in dark hue. Each box plot includes the biases of all stations at the respective environment and supersaturation. The numbers below show how many stations of the total in this category exhibit smaller absolute values of their bias. Outliers are indicated by black circles but do only occur in the continental group at low supersaturations.

https://doi.org/10.5194/egusphere-2026-1404
Preprint. Discussion started: 30 March 2026

Table A1. References to observation data and removed files during data checking. Please note: This table does not list missing files, but only the removed files during the process of data checking.

ID	Reference	Removed dates
ASI	Koontz et al. (2016b)	2016-04-25 to 2016-05-31, 2016-06-16, 2016-08-20, 2016-09-16 to 2016-11-16, 2017-01-19 to 2017-01-27, 2017-08-21
AWR	Koontz et al. (2016a)	2016-06-02, 2016-10-05, 2016-11-28, 2017-01-02 to 2017-01-03
COR	Koontz et al. (2018)	2018-10-18 to 2018-10-22, 2019-02-11 to 2019-02-12, 2019-03-10 to 2019-03-13, 2019-03-31 to 2019-04-09
ENA	Koontz et al. (2015)	2016-09-28 to 2016-09-29, 2016-11-11, 2017-07-28 to 2017-07-29, 2018-03-21 to 2018-03-23, 2018-12-08 to 2019-04-02, 2019-09-22 to 2020-10-26
NIM	Enekwizu et al. (2005a)	2006-03-22 to 2006-03-23, 2006-05-04 to 2006-08-11, 2006-09-04 to 2006-09-07
NSA	Andrews et al. (2007)	2008-02-24, 2008-05-07, 2008-05-12, 2008-05-25, 2009-02-28, 2009-05-07, 2009-05-27, 2010-01-22, 2010-02-08, 2011-04-05, 2011-04-08, 2011-04-11, 2011-05-06
OLI	Koontz et al. (2017a)	2019-06-07 to 2019-06-25, 2019-08-04, 2019-08-06
SGP	Enekwizu et al. (2006)	2007-05-22 to 2007-10-13, 2008-07-18, 2009-01-05, 2009-07-06 to 2009-07-10, 2009-05-15 to 2009-08-03
	Flynn et al. (2011)	2012-11-30 to 2013-06-11
	Koontz et al. (2011)	2012-11-30, 2012-12-01, 2013-03-02, 2013-06-12, 2013-06-19, 2013-07-03, 2016-01-17, 2016-03-04 to 2016-05-10, 2016-12-07
	Koontz et al. (2017b)	2017-08-22, 2017-11-27, 2018-04-16, 2018-06-01 to 2018-11-07, 2019-03-18 to 2019-03-21, 2019-03-28 to 2019-04-01, 2019-06-21 to 2019-07-01, 2019-07-12, 2019-09-24, 2019-11-16, 2020-11-17 to 2020-11-25, 2021-06-08 to 2021-06-10, 2021-07-12, 2021-09-21 to 2021-09-24, 2021-09-30 to 2021-10-04, 2021-10-18, 2021-10-23 to 2021-10-28, 2021-12-08

No dates needed to be removed for:
ATT (Pöhlker et al., 2016) and BRW, CES, FIK, JFJ, MEL, MHD, NOT, SEO, SMR, VAV (Petäjä et al., 2017) and FKB (Enekwizu et al., 2007), PYE (Enekwizu et al., 2005b), GRW (Shilling and Kulkarni, 2009), MAO (Flynn et al., 2014), PGH (Shilling and Kulkarni, 2011), PVC (Shilling and Kulkarni, 2012).

https://doi.org/10.5194/egusphere-2026-1404
Preprint. Discussion started: 30 March 2026

Table A2. Biases B [%] for all 25 stations at at all six supersaturations s, sorted by environment. Bold values indicate the best bias at each station.

ID	environment	$s = 0.1\,\%$	$s = 0.2\,\%$	$s = 0.4\,\%$	$s = 0.6\,\%$	$s = 0.8\,\%$	$s = 1.0\,\%$
ASI	remote marine	− 37.95	− **16.18**	+ 61.40	+ 121.14	+ 171.09	+ 221.79
ENA	remote marine	− 42.47	− **3.58**	+ 31.82	+ 85.49	+ 86.86	+ 103.53
GRW	remote marine	+ 11.53	− **5.84**	+ 17.90	+ 37.75	+ 63.02	+ 70.53
FIK	coastal	+ 786.67	+ 913.87	+ 26.05	+ **5.64**	+ 14.84	+ 26.00
MHD	coastal	− 68.91	− 30.61	+ **12.25**	+ 28.26	+ 35.85	+ 45.91
NOT	coastal	− 70.61	− 45.15	− **17.41**	+ 19.17	+ 45.28	+ 72.18
PVC	coastal	− 60.60	− 9.40	− 16.85	− 9.90	+ **2.00**	+ 6.99
PYE	coastal	+ **79.42**	+ 106.38	+ 84.65	+ 112.87	+ 132.81	+ 162.01
AWR	polar	+ **124.19**	+ 168.55	+ 215.42	+ 254.28	+ 245.72	+ 244.9
BRW	polar	− 55.46	− 21.48	− 16.61	− **4.59**	+ 13.68	+ 23.26
NSA	polar	− 80.36	− 52.74	− 42.89	− 23.62	− 15.76	− **2.73**
OLI	polar	+ **74.04**	+ 100.47	+ 141.39	+ 213.32	+ 214.81	+ 173.99
ATT	continental	− 67.31	− 39.13	+ **12.26**	+ 68.56	+ 119.68	+ 171.03
CES	continental	− 79.06	− 64.76	− 37.59	− 19.70	− **3.65**	+ 8.32
COR	continental	− ,58.45	− 70.93	− 65.53	− 58.73	− 56.41	− **51.16**
FKB	continental	+ 175.38	+ 66.93	− 18.23	+ **0.40**	+ 15.77	+ 29.17
JFJ	continental	− 63.44	− 60.34	− 51.72	− 42.87	− 35.38	− **32.05**
MAO	continental	+ 96.85	+ 581.05	+ **77.09**	+ 100.23	+ 170.80	+ 241.35
MEL	continental	− 75.79	− 68.46	− 47.60	− 31.96	− 23.63	− **16.02**
NIM	continental	+ 1619.24	+ 520.97	+ **76.65**	+ 78.78	+ 126.32	+ 137.04
PGH	continental	+ 75.79	+ 122.70	+ **23.61**	+ 29.08	+ 74.84	+ 134.42
SEO	continental	− 39.14	+ **11.53**	+ 69.68	+ 105.31	+ 143.3	+ 174.91
SGP	continental	− 59.43	− 45.98	− 41.90	− 33.40	− 25.06	− **13.34**
SMR	continental	− 69.68	− 62.42	− 40.99	− 28.42	− 18.59	− **10.06**
VAV	continental	− 21.59	− 47.78	− 28.40	− 10.07	+ **4.86**	+ 13.61

https://doi.org/10.5194/egusphere-2026-1404
Preprint. Discussion started: 30 March 2026

Author contributions. YEA and KB downloaded, prepared and processed observational as well as model data. MP provided measurement data for ATT. KB and JQ designed this study and provided scientific supervision. YEA conducted the statistical analysis, created plots and tables and drafted the initial manuscript. YEA and KB prepared and submitted the final manuscript with contributions from all co-authors. All authors edited the manuscript.

Competing interests. The authors declare no conflicts of interest relevant to this study.

Acknowledgements. The authors acknowledge data provision and data quality reporting from the Atmospheric Radiation Measurement (ARM; https://www.arm.gov) User Facility, a U.S. Department of Energy (DOE) Office of Science user facility managed by the Biological and Environmental Research Program. The authors also wish to acknowledge the ACTRIS (Aerosol, Clouds, and Trace Gases Research Infrastructure; http://www.actris.eu/) for its essential role in providing access to high-quality data, facilities, and technical support that were integral to the execution of this research. We further would like to acknowledge the World Data Centre for Climate (WDCC) for providing the CAMS-derived CCN data (https://doi.org/10.26050/WDCC/QUAERERE_CCNCAMS_v1).

KB and JQ acknowledge funding by the "WarmWorld project (FKZ 01LP1902C) funded by the German Ministry of Research, Technology and Space in its strategy "Research for Sustainability". JQ further acknowledges funding by the European Commission Horizon Europe grant "CleanCloud" (GA no 101137639).

https://doi.org/10.5194/egusphere-2026-1404
Preprint. Discussion started: 30 March 2026

References

Anders, Y., Block, K., and Quaas, J.: Validation of CAMS derived CCN variability with in-situ observations, Meteorologische Arbeiten (XXX) und Jahresbericht 2024 des Instituts für Meteorologie der Universität Leipzig, pp. 11–26, https://nbn-resolving.org/urn:nbn:de:bsz:15-qucosa2-1001574, 2025.

Andreae, M. O.: Correlation between cloud condensation nuclei concentration and aerosol optical thickness in remote and polluted regions, Atmospheric Chemistry and Physics, 9, 543–556, https://doi.org/10.5194/acp-9-543-2009, 2009.

Andrews, E., Enekwizu, O., Laskin, A., Hayes, C., and Uin, J.: Cloud Condensation Nuclei Particle Counter (AOSCCN), 2007-03-02 to 2011-08-30, North Slope Alaska (NSA), External Data (satellites and others) (X1), https://doi.org/10.5439/1988402, 2007.

Andrews, E., Zabala, I., Carrillo-Cardenas, G., Titos, G., Casquero-Vera, J. A., and Hallar, A. G.: Harmonized aerosol size distribution, cloud condensation nuclei, chemistry and optical properties at 10 sites, Scientific Data, 12, 937, https://doi.org/10.1038/s41597-025-04931-y, 2025.

Bellouin, N., Quaas, J., Gryspeerdt, E., Kinne, S., Stier, P., Watson-Parris, D., Boucher, O., Carslaw, K. S., Christensen, M., Daniau, A.-L., Dufresne, J.-L., Feingold, G., Fiedler, S., Forster, P., Gettelman, A., Haywood, J. M., Lohmann, U., Malavelle, F., Mauritsen, T., McCoy, D. T., Myhre, G., Mülmenstädt, J., Neubauer, D., Possner, A., Rugenstein, M., Sato, Y., Schulz, M., Schwartz, S. E., Sourdeval, O., Storelvmo, T., Toll, V., Winker, D., and Stevens, B.: Bounding Global Aerosol Radiative Forcing of Climate Change, Reviews of Geophysics, 58, e2019RG000 660, https://doi.org/https://doi.org/10.1029/2019RG000660, e2019RG000660 10.1029/2019RG000660, 2020.

Benedetti, A., Morcrette, J.-J., Boucher, O., Dethof, A., Engelen, R. J., Fisher, M., Flentje, H., Huneeus, N., Jones, L., Kaiser, J. W., Kinne, S., Mangold, A., Razinger, M., Simmons, A. J., and Suttie, M.: Aerosol analysis and forecast in the European Centre for Medium-Range Weather Forecasts Integrated Forecast System: 2. Data assimilation, Journal of Geophysical Research: Atmospheres, 114, https://doi.org/https://doi.org/10.1029/2008JD011115, 2009.

Block, K.: Cloud condensation nuclei (CCN) numbers derived from CAMS reanalysis EAC4 (Version 1), World Data Center for Climate (WDCC) at DKRZ, https://doi.org/10.26050/WDCC/QUAERERE_CCNCAMS_V1, 2023.

Block, K., Haghighatnasab, M., Partridge, D. G., Stier, P., and Quaas, J.: Cloud condensation nuclei concentrations derived from the CAMS reanalysis, Earth System Science Data, 16, 443–470, https://doi.org/10.5194/essd-16-443-2024, 2024.

Che, H., Stier, P., Watson-Parris, D., Gordon, H., and Deaconu, L.: Source attribution of cloud condensation nuclei and their impact on stratocumulus clouds and radiation in the south-eastern Atlantic, Atmospheric Chemistry and Physics, 22, 10 789–10 807, https://doi.org/10.5194/acp-22-10789-2022, 2022.

Choudhury, G. and Tesche, M.: A first global height-resolved cloud condensation nuclei data set derived from spaceborne lidar measurements, Earth System Science Data, 15, 3747–3760, https://doi.org/10.5194/essd-15-3747-2023, 2023.

Choudhury, G., Block, K., Haghighatnasab, M., Quaas, J., Goren, T., and Tesche, M.: Pristine oceans are a significant source of uncertainty in quantifying global cloud condensation nuclei, Atmospheric Chemistry and Physics, 25, 3841–3856, https://doi.org/10.5194/acp-25-3841-2025, 2025.

Cohard, J.-M., Pinty, J.-P., and Bedos, C.: Extending Twomey's Analytical Estimate of Nucleated Cloud Droplet Concentrations from CCN Spectra, Journal of the Atmospheric Sciences, 55, 3348–3357, https://doi.org/10.1175/1520-0469(1998)055<3348:ETSAEO>2.0.CO;2, 1998.

https://doi.org/10.5194/egusphere-2026-1404
Preprint. Discussion started: 30 March 2026

Deng, Z. Z., Zhao, C. S., Ma, N., Ran, L., Zhou, G. Q., Lu, D. R., and Zhou, X. J.: An examination of parameterizations for the CCN number concentration based on in situ measurements of aerosol activation properties in the North China Plain, Atmospheric Chemistry and Physics, 13, 6227–6237, https://doi.org/10.5194/acp-13-6227-2013, 2013.

Désalmand, F.: An Attempt to Characterize a Relationship between Supersaturation Spectrum, Size Spectrum and Solubility of CCN Observed over a Tropical Rain Forest, Journal of Atmospheric Sciences, 42, 472 – 477, https://doi.org/10.1175/1520-0469(1985)042<0472:AATCAR>2.0.CO;2, 1985.

Enekwizu, O., Hayes, C., and Uin, J.: Cloud Condensation Nuclei Particle Counter (AOSCCN), 2005-12-21 to 2007-01-07, ARM Mobile Facility (NIM), Niamey, Niger (M1), https://doi.org/10.5439/1988402, 2005a.

Enekwizu, O., Hayes, C., and Uin, J.: Cloud Condensation Nuclei Particle Counter (AOSCCN), 2005-03-04 to 2005-09-15, ARM Mobile Facility (PYE), Point Reyes, CA (M1), https://doi.org/10.5439/1988402, 2005b.

Enekwizu, O., Laskin, A., Hayes, C., and Uin, J.: Cloud Condensation Nuclei Particle Counter (AOSCCN), 2006-09-13 to 2011-03-09, Southern Great Plains (SGP), Central Facility, Lamont, OK (C1), https://doi.org/10.5439/1988402, 2006.

Enekwizu, O., Hayes, C., and Uin, J.: Cloud Condensation Nuclei Particle Counter (AOSCCN), 2007-03-19 to 2008-01-03, ARM Mobile Facility (FKB), Black Forest, Germany (M1), https://doi.org/10.5439/1988402, 2007.

Flynn, C., Shilling, J., and Kulkarni, G.: Aerosol Observing System (AOS): cloud condensation nuclei data, averaged (AOSCCNAVG), 2011-01-01 to 2014-09-29, Southern Great Plains (SGP), Central Facility, Lamont, OK (C1), https://doi.org/10.5439/1985586, 2011.

Flynn, C., Shilling, J., and Kulkarni, G.: Aerosol Observing System (AOS): cloud condensation nuclei data, averaged (AOSCCNAVG), 2014-07-01 to 2014-09-29, ARM Mobile Facility (MAO), Manacapuru, Amazonas, Brazil; AMF1 (M1), https://doi.org/10.5439/1985586, 2014.

Gryspeerdt, E. and Stier, P.: Regime-based analysis of aerosol-cloud interactions, Geophysical Research Letters, 39, https://doi.org/https://doi.org/10.1029/2012GL053221, 2012.

Gupta, H. V., Kling, H., Yilmaz, K. K., and Martinez, G. F.: Decomposition of the mean squared error and NSE performance criteria: Implications for improving hydrological modelling, Journal of Hydrology, 377, 80–91, https://doi.org/https://doi.org/10.1016/j.jhydrol.2009.08.003, 2009.

Holanda, B. A., Pöhlker, M. L., Walter, D., Saturno, J., Sörgel, M., Ditas, J., Ditas, F., Schulz, C., Franco, M. A., Wang, Q., Donth, T., Artaxo, P., Barbosa, H. M. J., Borrmann, S., Braga, R., Brito, J., Cheng, Y., Dollner, M., Kaiser, J. W., Klimach, T., Knote, C., Krüger, O. O., Fütterer, D., Lavrič, J. V., Ma, N., Machado, L. A. T., Ming, J., Morais, F. G., Paulsen, H., Sauer, D., Schlager, H., Schneider, J., Su, H., Weinzierl, B., Walser, A., Wendisch, M., Ziereis, H., Zöger, M., Pöschl, U., Andreae, M. O., and Pöhlker, C.: Influx of African biomass burning aerosol during the Amazonian dry season through layered transatlantic transport of black carbon-rich smoke, Atmospheric Chemistry and Physics, 20, 4757–4785, https://doi.org/10.5194/acp-20-4757-2020, 2020.

Hudson, J. G.: Relationship Between Fog Condensation Nuclei and Fog Microstructure, Journal of Atmospheric Sciences, 37, 1854 – 1867, https://doi.org/10.1175/1520-0469(1980)037<1854:RBFCNA>2.0.CO;2, 1980.

Hudson, J. G. and Yum, S. S.: Cloud condensation nuclei spectra and polluted and clean clouds over the Indian Ocean, Journal of Geophysical Research: Atmospheres, 107, https://doi.org/10.1029/2001JD000829, 2002.

Inness, A., Ades, M., Agustí-Panareda, A., Barré, J., Benedictow, A., Blechschmidt, A.-M., Dominguez, J. J., Engelen, R., Eskes, H., Flemming, J., Huijnen, V., Jones, L., Kipling, Z., Massart, S., Parrington, M., Peuch, V.-H., Razinger, M., Remy, S., Schulz, M., and Suttie, M.: The CAMS reanalysis of atmospheric composition, Atmospheric Chemistry and Physics, 19, 3515–3556, https://doi.org/10.5194/acp-19-3515-2019, 2019.

IPCC: The Earth's Energy Budget, Climate Feedbacks and Climate Sensitivity, p. 923–1054, Cambridge University Press, 2023.

https://doi.org/10.5194/egusphere-2026-1404
Preprint. Discussion started: 30 March 2026

Jayachandran, V. N., Varghese, M., Murugavel, P., Todekar, K. S., Bankar, S. P., Malap, N., Dinesh, G., Safai, P. D., Rao, J., Konwar, M., Dixit, S., and Prabha, T. V.: Cloud condensation nuclei characteristics during the Indian summer monsoon over a rain-shadow region, Atmospheric Chemistry and Physics, 20, 7307–7334, https://doi.org/10.5194/acp-20-7307-2020, 2020.

Ji, Q. and Shaw, G. E.: On supersaturation spectrum and size distributions of cloud condensation nuclei, Geophysical Research Letters, 25, 1903–1906, https://doi.org/10.1029/98GL01404, 1998.

Jia, H., Ma, X., Yu, F., and Quaas, J.: Significant underestimation of radiative forcing by aerosol–cloud interactions derived from satellite-based methods, Nature Communications, 12, 3649, https://doi.org/10.1038/s41467-021-23888-1, 2021.

Khvorostyanov, V. I. and Curry, J. A.: A simple analytical model of aerosol properties with account for hygroscopic growth: 1. Equilibrium size spectra and cloud condensation nuclei activity spectra, Journal of Geophysical Research: Atmospheres, 104, 2175–2184, https://doi.org/10.1029/98JD02673, 1999.

Khvorostyanov, V. I. and Curry, J. A.: Aerosol size spectra and CCN activity spectra: Reconciling the lognormal, algebraic, and power laws, Journal of Geophysical Research: Atmospheres, 111, 2005JD006 532, https://doi.org/10.1029/2005JD006532, 2006.

Khvorostyanov, V. I. and Curry, J. A.: Kinetics of Cloud Drop Formation and Its Parameterization for Cloud and Climate Models, Journal of the Atmospheric Sciences, 65, 2784 – 2802, https://doi.org/10.1175/2008JAS2606.1, 2008.

Kim, J. H., Yum, S. S., Shim, S., Yoon, S.-C., Hudson, J. G., Park, J., and Lee, S.-J.: On aerosol hygroscopicity, cloud condensation nuclei (CCN) spectra and critical supersaturation measured at two remote islands of Korea between 2006 and 2009, Atmospheric Chemistry and Physics, 11, 12 627–12 645, https://doi.org/10.5194/acp-11-12627-2011, 2011.

Koontz, A., Flynn, C., Andrews, E., Uin, J., Enekwizu, O., Hayes, C., and Salwen, C.: Cloud Condensation Nuclei Particle Counter (AOSCCN1COLAVG), 2011-08-10 to 2017-08-16, Southern Great Plains (SGP), Central Facility, Lamont, OK (C1), https://doi.org/10.5439/1255094, 2011.

Koontz, A., Flynn, C., Andrews, E., Uin, J., Enekwizu, O., Hayes, C., and Salwen, C.: Cloud Condensation Nuclei Particle Counter (AOSCCN1COLAVG), 2015-01-01 to 2020-10-28, Eastern North Atlantic (ENA), Graciosa Island, Azores, Portugal (C1), https://doi.org/10.5439/1255094, 2015.

Koontz, A., Flynn, C., Andrews, E., Uin, J., Enekwizu, O., Hayes, C., and Salwen, C.: Cloud Condensation Nuclei Particle Counter (AOSCCN1COLAVG), 2016-05-29 to 2017-01-03, ARM Mobile Facility (AWR), McMurdo Station Ross Ice Shelf, Antarctica; AMF2 (M1), https://doi.org/10.5439/1255094, 2016a.

Koontz, A., Uin, J., Andrews, E., Enekwizu, O., Hayes, C., and Salwen, C.: Cloud Condensation Nuclei Particle Counter (AOSCCN2COLAAVG), 2016-04-25 to 2017-10-30, ARM Mobile Facility (ASI), Ascension Island, South Atlantic Ocean; AMF1 (M1), https://doi.org/10.5439/1323894, 2016b.

Koontz, A., Uin, J., Andrews, E., Enekwizu, O., Hayes, C., and Salwen, C.: Cloud Condensation Nuclei Particle Counter (AOSCCN2COLAAVG), 2017-04-20 to 2019-09-06, Oliktok Point, AK, USA; Long-term Mobile Facility (OLI), Oliktok Point, Alaska; AMF3 (M1), https://doi.org/10.5439/1323894, 2017a.

Koontz, A., Uin, J., Andrews, E., Enekwizu, O., Hayes, C., and Salwen, C.: Cloud Condensation Nuclei Particle Counter (AOSCCN2COLAAVG), 2017-04-12 to 2026-01-21, Southern Great Plains (SGP), Lamont, OK (Extended and Co-located with C1) (E13), https://doi.org/10.5439/1323894, 2017b.

Koontz, A., Uin, J., Andrews, E., Enekwizu, O., Hayes, C., and Salwen, C.: Cloud Condensation Nuclei Particle Counter (AOSCCN2COLAAVG), 2018-09-24 to 2019-04-30, ARM Mobile Facility (COR), Cordoba, Argentina; AMF1 (main site for CACTI) (M1), https://doi.org/10.5439/1323894, 2018.

https://doi.org/10.5194/egusphere-2026-1404
Preprint. Discussion started: 30 March 2026

Kouvarakis, G., Tsigaridis, K., Kanakidou, M., and Mihalopoulos, N.: Temporal variations of surface regional background ozone over Crete Island in the southeast Mediterranean, Journal of Geophysical Research: Atmospheres, 105, 4399–4407, https://doi.org/https://doi.org/10.1029/1999JD900984, 2000.

Kulkarni, G., Mei, F., Sivaraman, C., Wang, J., Shilling, J. E., Newsom, R. K., Christensen, M. W., Berg, L. K., and Fast, J. D.: Assessment of Extinction-, Satellite-, and Model-Based Vertical Cloud Condensation Nuclei (CCN) Retrieval Methods Using Airborne CCN Measurements Over the Southern Great Plains, Journal of Geophysical Research: Atmospheres, 130, e2024JD042 565, https://doi.org/https://doi.org/10.1029/2024JD042565, e2024JD042565 2024JD042565, 2025.

Lance, S., Nenes, A., Medina, J., and Smith, J. N.: Mapping the Operation of the DMT Continuous Flow CCN Counter, Aerosol Science and Technology, 40, 242–254, https://doi.org/10.1080/02786820500543290, 2006.

Levy, R. C., Mattoo, S., Munchak, L. A., Remer, L. A., Sayer, A. M., Patadia, F., and Hsu, N. C.: The Collection 6 MODIS aerosol products over land and ocean, Atmospheric Measurement Techniques, 6, 2989–3034, https://doi.org/10.5194/amt-6-2989-2013, 2013.

Liu, J., Zheng, Y., Li, Z., and Cribb, M.: Analysis of cloud condensation nuclei properties at a polluted site in southeastern China during the AMF-China Campaign, Journal of Geophysical Research: Atmospheres, 116, https://doi.org/https://doi.org/10.1029/2011JD016395, 2011.

Martins, J. A., Gonçalves, F. L. T., Morales, C. A., Fisch, G. F., Pinheiro, F. G. M., Leal Júnior, J. B. V., Oliveira, C. J., Silva, E. M., Oliveira, J. C. P., Costa, A. A., and Silva Dias, M. A. F.: Cloud condensation nuclei from biomass burning during the Amazonian dry-to-wet transition season, Meteorology and Atmospheric Physics, 104, 83–93, https://doi.org/10.1007/s00703-009-0019-6, 2009.

Morcrette, J.-J., Boucher, O., Jones, L., Salmond, D., Bechtold, P., Beljaars, A., Benedetti, A., Bonet, A., Kaiser, J. W., Razinger, M., Schulz, M., Serrar, S., Simmons, A. J., Sofiev, M., Suttie, M., Tompkins, A. M., and Untch, A.: Aerosol analysis and forecast in the European Centre for Medium-Range Weather Forecasts Integrated Forecast System: Forward modeling, Journal of Geophysical Research: Atmospheres, 114, https://doi.org/https://doi.org/10.1029/2008JD011235, 2009.

Petäjä, T., Kulmala, M., Ovadnevaite, J., O'Dowd, C. D., Matsuki, A., Baltensperger, U., Herrmann, E., Bukowiecki, N., Kiendler-Scharr, A., Ogren, J., Prévôt, A. S. H., Slowik, J. G., Kanakidou, M., Wiedensohler, A., Nenes, A., Kristensson, A., Iwamoto, Y., Ehn, M., Liine Heikkinen, Schmale, J., Henning, S., Henzing, J. S., Keskinen, H., Sellegri, K., Bougiatioti, A., Kalivitis, N., Stavroulas, I., Jefferson, A., Minsu Park, Schlag, P., Pringle, K., Reddington, C., Aalto, P., Äijälä, M., Birmili, W., Paramonov, M., Fjæraa, A. M., Fiebig, M., Myhre, C. L., Frank, G., Swietlicki, E., Svennigsson, B., Cerina Wittbom, Fröhlich, R., Hammer, E., Gysel, M., Frumau, A., Kos, G., Kinochi, K., Ruper Holzinger, Mihalopoulos Nikolaos, Piccard, D., Poulain, L., Sonntag, A., Stratmann, F., Yum, S. S., Carslaw, K., Furuya, M., Hyono, H., and Tsurumaru, H.: Data from collocated observations of cloud condensation nuclei, particle size distributions, and chemical composition, https://doi.org/10.6084/M9.FIGSHARE.C.3471585.V1, 2017.

Pöhlker, M. L., Pöhlker, C., Ditas, F., Klimach, T., Hrabe de Angelis, I., Araújo, A., Brito, J., Carbone, S., Cheng, Y., Chi, X., Ditz, R., Gunthe, S. S., Kesselmeier, J., Könemann, T., Lavrič, J. V., Martin, S. T., Mikhailov, E., Moran-Zuloaga, D., Rose, D., Saturno, J., Su, H., Thalman, R., Walter, D., Wang, J., Wolff, S., Barbosa, H. M. J., Artaxo, P., Andreae, M. O., and Pöschl, U.: Long-term observations of cloud condensation nuclei in the Amazon rain forest – Part 1: Aerosol size distribution, hygroscopicity, and new model parametrizations for CCN prediction, Atmospheric Chemistry and Physics, 16, 15 709–15 740, https://doi.org/10.5194/acp-16-15709-2016, 2016.

Popp, T., De Leeuw, G., Bingen, C., Brühl, C., Capelle, V., Chedin, A., Clarisse, L., Dubovik, O., Grainger, R., Griesfeller, J., Heckel, A., Kinne, S., Klüser, L., Kosmale, M., Kolmonen, P., Lelli, L., Litvinov, P., Mei, L., North, P., Pinnock, S., Povey, A., Robert, C., Schulz, M., Sogacheva, L., Stebel, K., Stein Zweers, D., Thomas, G., Tilstra, L., Vandenbussche, S., Veefkind, P., Vountas, M., and Xue, Y.:

https://doi.org/10.5194/egusphere-2026-1404
Preprint. Discussion started: 30 March 2026

Development, Production and Evaluation of Aerosol Climate Data Records from European Satellite Observations (Aerosol_cci), Remote Sensing, 8, 421, https://doi.org/10.3390/rs8050421, 2016.

Pruppacher, H. R. and Klett, J. D.: Microphysics of clouds and precipitation, no. 18 in Atmospheric and oceanographic sciences library, Kluwer Academic Publishers, 2nd rev. and enl. ed edn., ISBN 978-0-7923-4211-3, 1997.

Quaas, J., Ming, Y., Menon, S., Takemura, T., Wang, M., Penner, J. E., Gettelman, A., Lohmann, U., Bellouin, N., Boucher, O., Sayer, A. M., Thomas, G. E., McComiskey, A., Feingold, G., Hoose, C., Kristjánsson, J. E., Liu, X., Balkanski, Y., Donner, L. J., Ginoux, P. A., Stier, P., Grandey, B., Feichter, J., Sednev, I., Bauer, S. E., Koch, D., Grainger, R. G., Kirkevåg, A., Iversen, T., Seland, Ø., Easter, R., Ghan, S. J., Rasch, P. J., Morrison, H., Lamarque, J.-F., Iacono, M. J., Kinne, S., and Schulz, M.: Aerosol indirect effects – general circulation model intercomparison and evaluation with satellite data, Atmospheric Chemistry and Physics, 9, 8697–8717, https://doi.org/10.5194/acp-9-8697-2009, 2009.

Quaas, J., Arola, A., Cairns, B., Christensen, M., Deneke, H., Ekman, A. M. L., Feingold, G., Fridlind, A., Gryspeerdt, E., Hasekamp, O., Li, Z., Lipponen, A., Ma, P.-L., Mülmenstädt, J., Nenes, A., Penner, J. E., Rosenfeld, D., Schrödner, R., Sinclair, K., Sourdeval, O., Stier, P., Tesche, M., van Diedenhoven, B., and Wendisch, M.: Constraining the Twomey effect from satellite observations: issues and perspectives, Atmospheric Chemistry and Physics, 20, 15 079–15 099, https://doi.org/10.5194/acp-20-15079-2020, 2020.

Rémy, S., Kipling, Z., Flemming, J., Boucher, O., Nabat, P., Michou, M., Bozzo, A., Ades, M., Huijnen, V., Benedetti, A., Engelen, R., Peuch, V.-H., and Morcrette, J.-J.: Description and evaluation of the tropospheric aerosol scheme in the European Centre for Medium-Range Weather Forecasts (ECMWF) Integrated Forecasting System (IFS-AER, cycle 45R1), Geoscientific Model Development, 12, 4627–4659, https://doi.org/10.5194/gmd-12-4627-2019, 2019.

Reutter, P., Su, H., Trentmann, J., Simmel, M., Rose, D., Gunthe, S. S., Wernli, H., Andreae, M. O., and Pöschl, U.: Aerosol- and updraft-limited regimes of cloud droplet formation: influence of particle number, size and hygroscopicity on the activation of cloud condensation nuclei (CCN), Atmospheric Chemistry and Physics, 9, 7067–7080, https://doi.org/10.5194/acp-9-7067-2009, 2009.

Roberts, G. C. and Nenes, A.: A Continuous-Flow Streamwise Thermal-Gradient CCN Chamber for Atmospheric Measurements, Aerosol Science and Technology, 39, 206–221, https://doi.org/10.1080/027868290913988, 2005.

Rose, D., Gunthe, S. S., Mikhailov, E., Frank, G. P., Dusek, U., Andreae, M. O., and Pöschl, U.: Calibration and measurement uncertainties of a continuous-flow cloud condensation nuclei counter (DMT-CCNC): CCN activation of ammonium sulfate and sodium chloride aerosol particles in theory and experiment, Atmospheric Chemistry and Physics, 8, 1153–1179, https://doi.org/10.5194/acp-8-1153-2008, 2008.

Schmale, J., Henning, S., Henzing, B., Keskinen, H., Sellegri, K., Ovadnevaite, J., Bougiatioti, A., Kalivitis, N., Stavroulas, I., Jefferson, A., Park, M., Schlag, P., Kristensson, A., Iwamoto, Y., Pringle, K., Reddington, C., Aalto, P., Äijälä, M., Baltensperger, U., Bialek, J., Birmili, W., Bukowiecki, N., Ehn, M., Fjæraa, A. M., Fiebig, M., Frank, G., Fröhlich, R., Frumau, A., Furuya, M., Hammer, E., Heikkinen, L., Herrmann, E., Holzinger, R., Hyono, H., Kanakidou, M., Kiendler-Scharr, A., Kinouchi, K., Kos, G., Kulmala, M., Mihalopoulos, N., Motos, G., Nenes, A., O'Dowd, C., Paramonov, M., Petäjä, T., Picard, D., Poulain, L., Prévôt, A. S. H., Slowik, J., Sonntag, A., Swietlicki, E., Svenningsson, B., Tsurumaru, H., Wiedensohler, A., Wittbom, C., Ogren, J. A., Matsuki, A., Yum, S. S., Myhre, C. L., Carslaw, K., Stratmann, F., and Gysel, M.: Collocated observations of cloud condensation nuclei, particle size distributions, and chemical composition, Scientific Data, 4, 170 003, https://doi.org/10.1038/sdata.2017.3, 2017.

Schmale, J., Henning, S., Decesari, S., Henzing, B., Keskinen, H., Sellegri, K., Ovadnevaite, J., Pöhlker, M. L., Brito, J., Bougiatioti, A., Kristensson, A., Kalivitis, N., Stavroulas, I., Carbone, S., Jefferson, A., Park, M., Schlag, P., Iwamoto, Y., Aalto, P., Äijälä, M., Bukowiecki, N., Ehn, M., Frank, G., Fröhlich, R., Frumau, A., Herrmann, E., Herrmann, H., Holzinger, R., Kos, G., Kulmala, M., Mihalopoulos, N., Nenes, A., O'Dowd, C., Petäjä, T., Picard, D., Pöhlker, C., Pöschl, U., Poulain, L., Prévôt, A. S. H., Swietlicki, E., Andreae, M. O., Artaxo,

https://doi.org/10.5194/egusphere-2026-1404
Preprint. Discussion started: 30 March 2026

P., Wiedensohler, A., Ogren, J., Matsuki, A., Yum, S. S., Stratmann, F., Baltensperger, U., and Gysel, M.: Long-term cloud condensation nuclei number concentration, particle number size distribution and chemical composition measurements at regionally representative observatories, Atmospheric Chemistry and Physics, 18, 2853–2881, https://doi.org/10.5194/acp-18-2853-2018, 2018.

Seinfeld, J. H., Bretherton, C., Carslaw, K. S., Coe, H., DeMott, P. J., Dunlea, E. J., Feingold, G., Ghan, S., Guenther, A. B., Kahn, R., Kraucunas, I., Kreidenweis, S. M., Molina, M. J., Nenes, A., Penner, J. E., Prather, K. A., Ramanathan, V., Ramaswamy, V., Rasch, P. J., Ravishankara, A. R., Rosenfeld, D., Stephens, G., and Wood, R.: Improving our fundamental understanding of the role of aerosol-cloud interactions in the climate system, Proceedings of the National Academy of Sciences, 113, 5781–5790, https://doi.org/10.1073/pnas.1514043113, 2016.

Shilling, J. and Kulkarni, G.: Aerosol Observing System (AOS): cloud condensation nuclei data, averaged (AOSCCNAVG), 2009-04-16 to 2010-12-30, ARM Mobile Facility (GRW), Graciosa Island, Azores, Portugal; AMF1 (M1), https://doi.org/10.5439/1985586, 2009.

Shilling, J. and Kulkarni, G.: Aerosol Observing System (AOS): cloud condensation nuclei data, averaged (AOSCCNAVG), 2011-06-09 to 2012-03-26, ARM Mobile Facility (PGH), ARIES Observatory, Nainital, Uttarkhand, India; AMF1 (M1), https://doi.org/10.5439/1985586, 2011.

Shilling, J. and Kulkarni, G.: Aerosol Observing System (AOS): cloud condensation nuclei data, averaged (AOSCCNAVG), 2012-07-16 to 2013-03-30, ARM Mobile Facility (PVC), Highland Center, Cape Cod MA; AMF1 (M1), https://doi.org/10.5439/1985586, 2012.

Spracklen, D. V., Carslaw, K. S., Pöschl, U., Rap, A., and Forster, P. M.: Global cloud condensation nuclei influenced by carbonaceous combustion aerosol, Atmospheric Chemistry and Physics, 11, 9067–9087, https://doi.org/10.5194/acp-11-9067-2011, 2011.

Stier, P.: Limitations of passive remote sensing to constrain global cloud condensation nuclei, Atmospheric Chemistry and Physics, 16, 6595–6607, https://doi.org/10.5194/acp-16-6595-2016, 2016.

Twomey, S.: The nuclei of natural cloud formation part II: The supersaturation in natural clouds and the variation of cloud droplet concentration, Geofisica pura e applicata, 43, 243–249, https://doi.org/10.1007/BF01993560, 1959.

Varghese, M., Prabha, T. V., Malap, N., Resmi, E., Murugavel, P., Safai, P., Axisa, D., Pandithurai, G., and Dani, K.: Airborne and ground based CCN spectral characteristics: Inferences from CAIPEEX – 2011, Atmospheric Environment, 125, 324–336, https://doi.org/10.1016/j.atmosenv.2015.06.041, 2016.

Wang, Y., Niu, S., Lu, C., Fan, S., Lv, J., Xu, X., Jin, Y., and Sun, W.: A new CCN activation parameterization and its potential influences on aerosol indirect effects, Atmospheric Research, 253, 105 491, https://doi.org/10.1016/j.atmosres.2021.105491, 2021.

Yum, S. S. and Hudson, J. G.: Vertical distributions of cloud condensation nuclei spectra over the springtime Arctic Ocean, Journal of Geophysical Research: Atmospheres, 106, 15 045–15 052, https://doi.org/https://doi.org/10.1029/2000JD900357, 2001.